

EOCENE BASIN RECORDS OF VOLCANISM, TOPOGRAPHY, AND
TECTONICS IN SOUTHERN BRITISH COLUMBIA, CANADA

A Thesis

Presented in Partial Fulfillment of the Requirements for the
Degree of Master of Science
with a

Major in Geology
in the
College of Graduate Studies
University of Idaho

by
Zachary S. Foster-Baril

Major Professor: Elizabeth Cassel, Ph.D.
Committee Members: Eric Mittelstaedt, Ph.D., Andrew Leier, Ph.D.
Department Administrator: Leslie Baker, Ph.D.

August 2017

Authorization to Submit Thesis

The thesis of Zachary S. Foster-Baril, submitted for the degree of Master of Science with a major in Geology and titled, "EOCENE BASIN RECORDS OF VOLCANISM, TOPOGRAPHY, AND TECTONICS IN SOUTHERN BRITISH COLUMBIA, CANADA," has been reviewed in final form. Permission, as indicated by the signatures and dates given below, is now granted to submit final copies to the College of Graduate Studies for approval.

Major Professor: _____ Date: _____

Elizabeth Cassel, Ph.D.

Committee Members: _____ Date: _____

Eric Mittelstaedt, Ph.D.

_____ Date: _____

Andrew Leier, Ph.D.

Department

Administrator: _____ Date: _____

Leslie Baker, Ph.D.

Abstract

The Eocene volcanic and sedimentary rocks of southwestern Canada preserve a complex record of extensional tectonics associated with the evolution of the western Cordillera hinterland. Potential mechanisms driving magmatism, rapid extension, and surface subsidence and uplift in the area include the opening of a slab window, slab rollback, and mantle lithospheric delamination. To test these models, this study combines stable isotope and elemental geochemistry, U/Pb geochronology, and stratigraphy of ignimbrites and sediments. New U/Pb zircon ages indicate basin sedimentation began prior to the initiation of an ignimbrite flare-up event in the south at ~53 Ma and propagating northward through 51 Ma. A regional unconformity and terrestrial sedimentation followed the end ignimbrite flare-up event at ~47 Ma. δD_{glass} values from ignimbrites represent Eocene meteoric water isotope compositions, which correlate with depositional environment. Precipitation-hydrated units have δD_{glass} values of -186.5‰ and -197.3‰ $\pm 2.5\%$. In comparison to a previously reported near shore value $\delta D_{\text{precipitation}}$ of -55 $\pm 2\%$, these values indicate a high standing (2800-3000 m ± 300 m) hinterland existed synchronously with the regional ignimbrite flare-up, sedimentation, and core complex extension. Enriched δD_{glass} values from glasses deposited in lacustrine systems reflect local evaporation, likely enhanced during the Early Eocene Climatic Optimum. The formation of a slab window is the most likely mechanism driving early to middle Eocene magmatism and basin accumulation within the southern Canadian Cordillera hinterland.

Acknowledgements

I would like to thank Dr. Elizabeth Cassel for her expert guidance. I would also like to thank my committee members Dr. Eric Mittelstaedt and Dr. Andrew Leier for their support. I am grateful for the guidance and support from my collaborators including Dr. Jeff Vervoort, Dr. Bruce Archibald, Dr. Scott Boroughs, Dr. Tom Williams, and Charles Knaack. Thanks to my fellow graduate students including Emily White, Andrew Canada, Jeff Larimer, and Tom Morrow. I thank Kevin Townsley and Eric Stauffer for the support in the field and the lab. Special thanks to Alex Johnson for the insightful comments and critiques of this work. Funding for this project was provided by the Geological Society of America, Geological Society of America-Rocky Mountain Section, Society for Sedimentary Geology-Rocky Mountain Section, and the University of Idaho-College of Science.

Dedication

Thanks to my family and friends for supporting me over the years.

Table of Contents

Authorization to Submit Thesis	ii
Acknowledgements	iv
Dedication	v
Table of Contents	vi
List of Tables	viii
List of Figures	ix
List of Appendices	x
1.0 Introduction	1
2.0 Regional Geology	3
2.1 Paleoelevation Reconstructions	6
2.2 Potential Geodynamic Models	8
3.0 Methodology	11
3.1 Stratigraphy	11
3.2 Volcanic Glass Stable Isotope Analyses	11
3.3 Paleoaltimetry Model	12
3.4 Trace and Rare Earth Elemental Analyses	13
3.5 U/Pb Geochronology	14
4.0 Results	15
4.1 Stratigraphic Characteristics	15
4.1.1 Princeton Group – Allenby Formation – Hardwick Sandstone	15
4.1.2 Kamloops Group – Tranquille Formation – McAbee Beds	16
4.1.3 Penticton Group – White Lake Formation	17
4.2 Field Occurrences and Sample Descriptions of Ignimbrites and tuffs	19
4.3 Geochemical Correlation of Ignimbrites	21
4.4 U/Pb Radiometric Dating	22
4.5 δD_{glass} Analytical Results and Paleoaltimetry Model	23
5.0 Discussion	26
5.1 Stratigraphic Interpretations	26
5.1.1 Princeton Group – Allenby Formation – Hardwick Sandstone	26
5.1.2 Kamloops Group – Tranquille Formation – McAbee Beds	26

5.1.3 Penticton Group – White Lake Formation.....	27
5.2 Ignimbrite Geochemistry and Correlation.....	29
5.3 Hydrogen Isotope Ratios in Hydrated Volcanic Glass.....	31
5.4 Potential Tectonic Mechanisms	33
6.0 Conclusions.....	35
7.0 References.....	38

List of Tables

Table 2.1. Previous Age Assignments of Regional Volcanic and Sedimentary Strata.....	7
Table 4.1. Hardwick Sandstone Lithofacies Descriptions and Depositional Environments...	16
Table 4.2. McAbee Beds Lithofacies Descriptions and Depositional Environments.....	17
Table 4.3. White Lake Lithofacies Descriptions and Depositional Environments.....	18
Table 4.4. $^{238}\text{U}/^{206}\text{Pb}$ Age Determinations of Zircons.....	23
Table 4.5. Measured $\delta\text{D}_{\text{glass}}$ Values.....	24

List of Figures

Figure 2.1. Regional Geologic Map.....	47
Figure 2.2. Eocene Plate Tectonic Reconstructions.....	48
Figure 2.3. Regional Stratigraphy and Nomenclature.....	49
Figure 2.4. Potential Geodynamic Mechanisms.....	50
Figure 4.1. Regional Geologic Map with Results.....	51
Figure 4.2. Generalized and Correlated Stratigraphy.....	52
Figure 4.3. Photos of Stratigraphic Sections.....	53
Figure 4.4. Trace and Rare Earth Elemental Analytical Results.....	54
Figure 4.5. $^{238}\text{U}/^{206}\text{Pb}$ Radiometric Dating Results.....	55
Figure 4.6. Regional Stratigraphy with Results.....	56
Figure 5.1. Model Calibration and Modeled Eocene Paleoelevation.....	57

List of Appendices

Appendix 1. White Lake, McAbee Beds, and Hardwick Sandstone Stratigraphy.....	58
Appendix 2. Trace and Rare Earth Elemental Analyses Results.....	62
Appendix 3. Petrographic Glass Images with Descriptions.....	63
Appendix 4. $^{238}\text{U}/^{206}\text{Pb}$ Radiometric Dating Results.....	65
Appendix 5. Cathodoluminescence Images of Zircon Grains.....	74

1.0 Introduction

Changes in surface topography directly reflect mantle-crust interactions and plate boundary dynamics (Wernicke et al., 1996; Chamberlain et al., 2012). In southern British Columbia, a series of early Eocene basins record subsidence, volcanism, surface deformation, and metamorphic core complex formation at the onset of orogenic collapse. Although the paleobotany of these basins is well-characterized, a lack of precise age dating and stratigraphic correlations limit understanding of the sequence of events, relationships between sedimentation and volcanism, and the potential drivers for Eocene landscape evolution. Proposed mechanisms focus primarily on the volcanic record, and include the opening of a slab window following the subduction of a triple junction (Haeussler et al., 2003; Breitsprecher, 2003), rollback of the Farallon slab (Humphreys, 2009; Chamberlain et al., 2012), or delamination of mantle lithosphere (Bao et al., 2014). Each tectonic mechanism will affect the surface elevations differently and alter the composition and distribution of volcanics and the timing of an ignimbrite flare-up events (Breitsprecher et al., 2003; Brun and Faccenna, 2008; Smith et al., 2014; DeCelles, 2015).

Numerous widespread ignimbrites and tuffs are present throughout the study area, but post-depositional normal and dextral faulting have made local and regional correlation difficult (Read, 2000). Fluvial and lacustrine strata and interbedded ignimbrites and tuffs unconformably overlie early Eocene basalt to rhyolite flows and underlie late Eocene volcanic breccias and effusive basaltic flows (Ewing, 1981; Read, 2000). Eocene volcanic rocks are calc-alkaline and show chemical signatures indicative of an unusually primitive source melt. Adakite signatures are found throughout the region, but the mechanism producing this signature is still debated. Previous age assignments based on sparse K/Ar (whole rock, hornblende, and micas) and U/Pb (zircon) radiometric dating indicate that regional sedimentation occurred between 53.1 ± 1.5 Ma and 45.2 ± 1.1 Ma (e.g., Hills and Baadsgaard, 1967; Ickert et al., 2007), but correlation of sedimentary and volcanic units between individual basins is still unconstrained due to the lack of dating within many of these basins.

Previous Eocene elevation estimates in the region were based on paleoflora and $\delta^{18}\text{O}$ values from carbonate and muscovite and were commonly sampled at a single location. Interpreted elevations range from 1.6-4.9 km (Smith, 2009; Mulch et al., 2007; Mix et al.,

2011). Sparse and imprecise age constraints on strata, wide ranging paleoaltimetry estimates, and inconsistent geochemical data from volcanic strata have hindered researchers from forming a regionally unifying tectonic and basin history.

We combine stratigraphy and lithofacies analysis with trace and rare earth element (TREE) glass geochemistry, new zircon U/Pb radiometric ages, and hydrogen isotope ratios (δD) of hydrated volcanic glass from interbedded ignimbrites and tuffs to determine the timing and magnitude of elevation changes, the spatial and temporal geochemical evolution of volcanic rocks, and the timing of sedimentation in the southern Canadian Cordillera hinterland. This study describes twelve geochemically distinct ignimbrite and tuffs units from the Princeton and Kamloops Basins. New U/Pb ages indicate deposition of the McAbee beds, Falkland sediments, and the oldest sediments within the Princeton Group occurred during the Early Eocene Climatic Optimum (EECO) and provide a terrestrial climate record of this period of high pCO_2 (600 ppm to >1,300 ppm) and high temperatures (12°C warmer than modern) (Smith et al., 2010; Beerling and Royer, 2011). In addition, new paleoaltimetry data indicates that these basins formed at high elevations between 50 Ma and ~47 Ma. Following the most recent reclassification of the adakite geochemical signature, five of the sixteen previously reported adakite samples are now classified as adakite, while this study identifies one additional adakite from the Princeton basin based on glass TREE geochemical signatures.

2.0 Regional Geology

The southern Canadian Cordillera, a product of Paleozoic to Paleocene collisional tectonics along the western margin of North America, is divided into four morphogeological belts (Fig. 2.1) (Price, 1994; Monger and Price, 2002; Dickinson, 2004; Simony and Carr, 2011). The westernmost igneous and metamorphic rocks of the Coast Belt represent the accreted material and remnant volcanic arc associated with the subduction of one or more oceanic plates (Farallon, Kula, and Resurrection) under the North American Plate beginning in the Mid-Jurassic (Fig. 2.2) (Monger et al., 1982; Price, 1986; Haeussler et al., 2003; Simony and Carr, 2011). Fold and thrust deformation in the easternmost rocks of the Omineca and the Foreland belts record ~50% crustal shortening between the Mid-Jurassic to Late Cretaceous (Price and Mountjoy, 1970; Coney and Harms, 1984; Simony and Carr, 2011). Coney and Harms (1984) posited that a proportional isostatic response to this shortening resulted in increased paleoelevations in the hinterland to ~4 km (Bardoux and Mareschal, 1994). Arc magmatism ceased in the latest Cretaceous, as indicated by the presence of only rare latest Cretaceous to Paleocene plutons in the Coast Belt and southern Intermontane Belt (Armstrong, 1988). In the Paleocene to Eocene, the compressional regime transitioned to extensional and transtensional forces, as recorded by core complex exhumation, basin formation, and inboard volcanism within the Intermontane Belt (e.g., Ewing, 1981; Monger, 1985; Parrish et al., 1988; Brown et al., 2012).

Thermochronology from monazite, zircon, hornblende, and mica indicate two stages of cooling during the formation of the metamorphic core complexes in southern British Columbia and northern Washington. (Vanderhaeghe et al., 2002; Laberge and Pattison, 2007; Gordon et al., 2008; Cubley et al., 2013). This mineral suite records the first stage of cooling from 700 to 300°C between ~65 to ~48 Ma, an average rate of 24°C/my (Vanderhaeghe et al., 2002; Laberge and Pattison, 2007; Cubley et al., 2013). U/Pb dating of monazite and zircon rims indicates that crystallization (~700-800°C) of leucogranites and initiation of core complex extension occurred between ~65 and ~56 Ma (Gordon et al., 2008). $^{40}\text{Ar}/^{39}\text{Ar}$ apparent ages from hornblende indicate cooling through ~500°C occurred between ~59 and ~54 Ma (Vanderhaeghe et al., 2002). Overlapping mean ages of muscovite and biotite (between ~52 and ~48 Ma) indicate cooling from 350°C to 300°C occurred rapidly (Vanderhaeghe et al., 2002; Laberge and Pattison, 2007). Apatite fission track ages and

diffusion domains of K-feldspar and zircon indicate a second slower cooling event from 300°C to 100°C occurred between ~45 and ~33 Ma, an average rate of 17°C/my (Vanderhaeghe et al., 2002; Laberge and Pattison, 2007; Gordon et al., 2008; Cubley et al., 2013).

A series of Eocene basins consisting of interbedded volcanic and clastic sedimentary rocks, referred to as the Challis-Kamloops basins record three main phases of volcanism and rapid sedimentation during the onset of extension (Ewing, 1981; Monger, 1985; Parrish et al., 1988; McClaughry and Gaylord, 2005; Brown et al., 2010). The nomenclature of the interbedded volcanic and clastic strata is highly varied and dependent on the specific locality. In southern British Columbia to northern Washington, the strata are split into the Kamloops, Penticton, Princeton, and Republic Groups (Table 2.1; Fig. 2.3). The earliest stage of synextensional deposition (~53 Ma) includes breccia, conglomerate, and sandstone of the Kettle River Formation, O'Brien Creek Formation, and Springbrook Formation (Pearson and Obradovich, 1977; Rittenhouse-Michell, 1997). Unconformably overlying the earliest sedimentary strata is a ~2 km thick suite of andesite, basalt, and minor rhyolite of the Arlington Formation, Thompson Assemblage, Marama Formation, Marron Formation, and Cedar Formation. Deposition of these units occurred between ~53 to ~48 Ma (Pearson and Obradovich, 1977; Ewing, 1981; Church, 1985). A ~1-3 km thick suite of fluvial and lacustrine sedimentary rocks interbedded with ignimbrites of andesitic to rhyolitic composition unconformably overlie the earliest volcanic formations and comprise the Sanpoil, Allenby, White Lake, and Tranquille Formations. Deposition of these formations occurred between ~52 and 46 Ma. (Rouse and Mathews, 1961; Hills and Baadsgaard, 1967; Pearson and Obradovich, 1977; Atwater and Rinehart, 1984; Read, 2000; Villeneuve and Mathewes, 2005; Ickert et al., 2007). The upper Klondike, Skaha, Battle Creek, and Dewdrop Flats Formations comprise the youngest known Eocene units, and include volcanoclastic breccia, conglomerate, sandstone, and local andesite, basalt, and minor rhyolite estimated to be ca. 49 – 41 my old (Ewing, 1981; Pearson and Obradovich, 1977; Read, 2000).

Previous investigations of Eocene stratigraphy were focused on the easternmost Penticton and Republic Groups, located adjacent to the core complexes (Church, 1973; Pearson and Obradovich, 1977; Suydam and Gaylord, 1997; McClaughry and Gaylord, 2005). Clasts of schist and gneiss from the core complex footwalls are found within the

youngest Skaha and Klondike Formations of these basins (Suydam and Gaylord, 1997; McClaughry and Gaylord, 2005). Based on the presence of footwall metamorphic clasts, syndepositional extension, and the formation of rotated grabens and half grabens, researchers determined that sedimentation of the Republic and Penticton Groups occurred during the development of supradetachment basins (Suydam and Gaylord, 1997; McClaughry and Gaylord, 2005). Supradetachment basins provide a more complete record of the timing and relations of core complex exhumation than just thermochronologic data (McClaughry and Gaylord, 2005). To the west, the Princeton and Kamloops Groups also provide a record of synextensional graben and half graben development (Ewing, 1981; Read, 2000). The prevalence of Eocene shear zone complexes, however, indicates the possibility of more strike-slip influence during the development of these basins than in a supradetachment basin (Ewing, 1981; Read, 2000). A detailed account of basin development and sediment deposition has yet to be determined.

Syndepositional and synextensional volcanic rocks are prevalent throughout the region. The Kamloops, Princeton, Penticton, Colville volcanic suites are composed of calc-alkaline basalt to rhyolite and reach a maximum combined thickness of 1,500 m (Pearson and Obradovich, 1977; Ewing, 1981; Morris et al., 1999; Read, 2000; Dostal et al., 2003; Ickert et al., 2007). Alkalinity (K_2O/SiO_2) increases from moderate levels (~ 0.05) in the north to high levels in south (~ 0.14), consistent with a transition from alkali-arc affinities in the north to intraplate affinities in the south (Breitsprecher et al., 2003). More mature compositions likely formed due to fractional crystallization of variable parental magmas (Ewing, 1981; Morris et al., 1999). The ages of the formations comprised of primarily volcanic rocks are between ~ 48 and ~ 52 Ma, but these constraints are based mostly on dating conducted within the formations composed of interbedded sedimentary rocks and ignimbrites (e.g., Pearson and Obradovich, 1977; Ickert et al., 2007). In addition, the uncertainties reported on the $^{40}Ar/^{39}Ar$ analyses of any mineral except sanidine are smaller than absolute uncertainties (Smith et al., 2008).

Based on the criteria presented in Defant and Drummond (1990), sixteen samples from the Princeton, Kamloops, and Penticton Groups show adakite signatures (Breitsprecher et al., 2003; Ickert et al., 2007). Adakite signatures are commonly used as an important line of evidence for the interpretation of tectonic models. Adakites are defined as intermediate- to

high-silica rocks with high Sr/Y and La/Yb ratios and low Y and Yb concentrations. Possible mechanisms to make adakite signatures include the delamination of garnet-bearing crustal rocks into the mantle, subduction erosion, or partial melting of emplaced arc basalts due to upwelling asthenosphere (e.g., Kay, 1978; Gao et al. 2004; Macpherson and Hall, 2002). Trace element modeling shows the adakite signature found in southern Canada is due to Eocene reheating of the basaltic dykes emplaced during the Mesozoic (Ickert et al., 2007). But the source of the heat needed to create these adakite signatures is still unknown (Ickert et al., 2007). The upwelling of asthenosphere provided by slab rollback, a slab window, or mantle lithosphere delamination could produce enough heat to trigger the partial melting necessary to produce adakite signatures in volcanic rocks (Fig. 2.4; Thorkelson and Breitsprecher, 2005; Gao et al., 2007).

2.1 Paleoelevation Reconstructions

Regional Eocene sedimentary strata provide a terrestrial record of paleoclimatic conditions during the EECO and Middle Eocene Climatic Optimum, which can be used to estimate paleotemperature gradients and past elevations (Smith et al., 2009). Taxa indicating frost-free tropical and subtropical environments are present at mid-latitudes including the southern Canadian Cordillera during the Eocene (Wolfe and Wehr, 1987; Wing and Greenwood, 1993; Greenwood and Wing, 1995; Archibald and Mathews, 2000). Estimates of Eocene mean annual temperature (MAT) within the Intermontane Belt, determined based on leaf physiognomy and leaf margin analysis, range from $8.3 \pm 2^\circ\text{C}$ to $13.0 \pm 3.1^\circ\text{C}$ (Wolfe, 1994; Wolfe, 1998; Greenwood et al., 2005; Smith et al., 2009). The early Eocene Puget Group of Washington State, a locality near the paleoshoreline, records a MAT of $18.2 \pm 2^\circ\text{C}$ (Wolfe et al., 1998). The estimated regional terrestrial temperature lapse rate for western North America during the Eocene is $3.0^\circ\text{C}/\text{km}$ (Wolfe et al., 1998). Using a temperature difference of 5.1°C from CLAMP-derived paleobotanical studies, Smith et al. (2009) estimated that the Eocene paleoelevation of southern British Columbia was 2.2 ± 1.3 km. But the precision of the MAT estimates by CLAMP-derived paleobotany methods is underestimated by at least $\pm 1.2^\circ\text{C}$ due to leaf area bias and may produce additional uncertainties of ± 1.2 km in paleoelevation estimates (Peppe et al., 2010). Adding this additional uncertainty provides an estimated paleoelevation of southern British Columbia of

2.2 +/-2.5 km. Eocene sedimentary strata also contain records of sediment provenance and paleoflow, which can provide insights into regional relief and relative paleoelevations.

Table 2.1. Previous Age Assignments of Regional Volcanic and Sedimentary Strata

Group	Formation or Unit	Latitude (°N)	Longitude (°W)	Dating Method [Mineral]	Age (Ma)	± 2σ Error	Standard	Source
Republic	Klondike Mountain	48.916	118.794	K/Ar [Biotite]	49.1	1.7	NA	Pearson and Obradovich (1997)
		48.916	118.794	K/Ar [Biotite]	48.1	1.4		
		48.916	118.794	K/Ar [Biotite]	47.4	1.6		
		48.916	118.816	K/Ar [Hornblende]	41.4	1.5		
		48.916	118.816	K/Ar [Hornblende]	41.3	2		
	Sanpoil	48.513	118.741	K/Ar [Biotite]	52.1	1.7		
		48.577	188.632	K/Ar [Biotite]	51.2	1.7		
48.577		118.631	K/Ar [Plagioclase]	48.4	3			
O'Brien Creek	48.382	117.239	K/Ar [Biotite]	53.1	1.5			
Penticton	Marron	NA	NA	K/Ar [NA]	49	NA	Mathews (1946)	
		NA	NA	K/Ar [Biotite]	51.6	1.8	Church (1973)	
		49.828	119.740	K/Ar [Biotite]	52.9	3.6	Dostal et al. (2003)	
		49.550	119.867	K/Ar [Biotite]	52.7	3.0		
	49.300	119.6167	K/Ar [Biotite]	52.5	3.6			
White Lake	49.300	119.6167	K/Ar [Biotite]	52.5	3.6			
Princeton	Summers Creek	49.572	120.501	K/Ar [Biotite]	46.2	1.9	Read (2000)	
	Jura Andesite	49.586	120.484	K/Ar [Whole Rock]	49.4	2		
	Lower Nicola	49.148	120.883	⁴⁰ Ar/ ³⁹ Ar [Hornblende]	48.1	2.3	Fish Canyon Tuff	Ickert et al. (2007)
	Friday Creek	49.188	120.785	⁴⁰ Ar/ ³⁹ Ar [Hornblende]	49.7	1.7		
	Fig Lake	NA	NA	⁴⁰ Ar/ ³⁹ Ar [Hornblende]	50.0	1.6		
	Boss Lake	49.893	120.785	⁴⁰ Ar/ ³⁹ Ar [Whole Rock]	50.2	0.4		
	Agate Mountain	49.383	120.407	⁴⁰ Ar/ ³⁹ Ar [Ground mass]	51.7	1.6		
	Quilchena Creek Tuff	50.128	120.506	⁴⁰ Ar/ ³⁹ Ar [Sanidine]	51.5	0.3		
Quilchena Creek Tuff	50.128	120.506	²³⁸ U/ ²⁰⁶ Pb [Zircon]	52.8	2.53			
Kamloops	McAbee	50.800	121.167	K/Ar [Plagioclase]	49	2	NA	Hills and Baadsgaard (1967), recalculated by Ewing (1981)
				K/Ar [Biotite]	51	2		
				K/Ar [Plagioclase]	52	2		
	Monte Lake (Falkland)	50.493	119.831	K/Ar [Whole Rock]	50.5	1.8		

A study on paleophysiography and paleodrainage directions in southern British Columbia suggests a base level reduction of ~1 km between the Cretaceous and middle Eocene (Tribe, 2005). Excluding minor changes due to glacial incision in the Quaternary, the base level elevation and relief remain unchanged since the middle Eocene (Tribe, 2005). But analyses of δD_{water} from recrystallized muscovite in the Shuswap and Kettle metamorphic core complexes show depleted waters between $-115 \pm 5\text{‰}$ and $-157 \pm 5\text{‰}$ from extensional faults between ~49 and ~47 Ma (Mulch et al., 2007). It is possible this large range reflects magmatic water infiltrating the extensional faults (Mulch et al., 2007). Mulch et al. (2007) used a modeled Eocene lapse rate based on Eocene relative humidity and sea surface temperatures from Huber and Caballero (2003) to estimate middle Eocene elevations of the Omineca Belt between 4,963 m (+1,087 m/-630 m) and 4,227 m (+1,054 m/-833 m). It is important to note that this isotopic lapse rate is not calibrated for southern British Columbia. Analysis of one carbonate sample from Eocene strata in the Princeton Group provided a $\delta^{18}\text{O}$ value of $-19.7 \pm 1.7\text{‰}$, an approximate $\delta D_{\text{precip.}}$ value of $-147.6 \pm 13.1\text{‰}$ (Mix et al., 2011). Using a regional paleotemperature estimate from Huber and Caballero (2003) to model an unreported isotopic lapse rate, Mix et al. (2011) calculated a paleoelevation estimate of 4,200 m (+758 m/-487 m). Terrestrial $p\text{CO}_2$ estimates in the region range from 600 ppm to >1,300 ppm and agree with marine benthic phytoplankton estimates (Smith et al., 2010; Beerling and Royer, 2011). Increasing $p\text{CO}_2$ could reduce the isotopic lapse rate up to ~8.1‰/km leading to the large underestimation of isotopic-based elevation reconstructions (Poulsen and Jeffery, 2011).

High early Eocene paleoelevation estimates in conjunction with shifts over time in younger isotopic records from Montana, Wyoming, and Nevada led Mix et al. (2011) and other researchers to suggest a surface uplift wave propagated southward from B.C. throughout the Eocene due to Farallon slab rollback (Mulch et al., 2007; Chamberlain et al., 2012). A surface uplift wave of <1 km could be hidden within the isotopic record and a more precise modeling approach is needed (Chamberlain et al., 2012).

2.2 Potential Geodynamic Models

Previous researchers proposed three potential end-member models for the early Eocene crustal and mantle processes that drove the observed volcanic and sedimentary

patterns in the region. The potential evidence needed to discern the possible influence of each process on the alteration of the Eocene landscape is discussed below (Fig. 2.4):

- 1) Formation of a slab window (Thorkelson, 1996; Haeussler et al., 2003; Breitsprecher, 2003; Dostal et al., 2003; Ickert et al., 2007).

A number of studies use evidence from paleomagnetic anomalies from oceanic plates and arc volcanics to infer that two or more plates and a northward propagating spreading-ridge system were subducted under the southern Canadian Cordilleran region of the North American plate by ~56 Ma (Atwater, 1970; Thorkelson and Taylor, 1989; Breitsprecher, 2003). This would have formed a propagating slab window that allowed hot asthenosphere to interact with the lower lithosphere, causing rapid uplift in the Coast Mountains and the Intermontane Belt (Hollister, 1982). Hollister (1982) estimated an uplift rate of 2 mm/yr in the Coast Mountains between 62 and 48 Ma. Diagnostic features of slab windows include: 1) anomalous compositions and locations of arc volcanism, or cessation of arc magmatism, 2) arc-like compositions north of the proposed slab window, 3) near synchronous, voluminous, extension-style alkaline arc magmatism with adakite signatures, and 4) short term uplift in the back-arc above the slab window (Haeussler; 2003). Expected basin features include 1) formation of initially segmented basins in a back-arc setting evolving into regional depositional centers, and 2) a south to north succession of basin initiation following the propagation of the proposed slab window. Stratigraphic features include a progression from fluvial and lacustrine lithofacies to alluvial lithofacies followed by a large regional unconformity.

- 2) Slab rollback of the Farallon Plate (e.g., Humphreys, 2009; Chamberlain et al., 2012; Smith et al., 2014)

To the south of the study area, in the western U.S., it is well documented that rollback of the shallow to flat Farallon slab caused a southwestward progression of volcanism, basin formation, and reconfiguration of drainage divides from ca. 56 – 24 my ago (e.g., Carroll and Bohacs, 1999; Göğüş and Pysklywec, 2008). Some Eocene plate reconstructions include a Farallon slab extending northward beneath the study region, with the plate boundary as far north as Alaska (e.g., Haeussler et al., 1995). If this was

the Eocene plate configuration, then slab rollback would have preceded or been synchronous with the documented rollback in the western United States. Potential evidence for slab rollback would include: 1) the cessation of arc magmatism within the Coast Belt during shallowing in the Late Cretaceous, and reinitiation of volcanism during rollback to the east of the arc in the Intermontane and Omineca Belts, 2) the progression of topographic uplift and voluminous volcanism from north to south due to upwelling asthenosphere following slab removal, and 3) the initiation of core complex extension (Brun and Faccenna, 2008). Typical inboard volcanism during slab rollback includes tens of explosive eruptions of andesite, dacite, and rhyolite type magmas (Best et al., 2016). Diagnostic stratigraphic characteristics include a progression from fluvial to lacustrine lithofacies followed by volcanic and volcanoclastic sedimentation and finally a regional unconformity (Smith et al., 2014).

3) Lithospheric delamination (Bao et al., 2014)

Bao et al. (2014) use a positive anomaly in Rayleigh-wave tomographic data and thermochronological data to interpret a delamination event commencing at ~55 Ma in southern British Columbia. DeCelles et al. (2009) theorized the following cyclical cordilleran events: crustal shortening and proportional crustal thickening within the hinterland initiates a high flux arc magmatic event within the arc and hinterland. Concurrently, regional subsidence occurs due to the negative buoyancy on the upper plate exerted by the growing eclogite root. The eclogite root reaches a critical mass causing synchronous foundering and whole-sale removal of the lower lithosphere, rapid surface uplift in the hinterland (>1 km), and an ignimbrite flare-up event caused by the rising hot asthenosphere. Paleoelevations in the hinterland should be at lower elevations at the initiation of the ignimbrite flare-up event (DeCelles et al., 2009). Volcanism in the hinterland is localized to the area of delamination with ocean island basalt and arc-like geochemical signatures (Ducea et al., 2013). Diagnostic basin characteristics include initially slow subsidence and basin accumulation with the absence of bounding fault systems, followed by rapid short-lived subsidence, evidenced by basin inversion dominated by lacustrine lithofacies and the absence of wedge-top, rift, intra-arc, or strike-slip basins (DeCelles et al., 2015).

3.0 Methodology

3.1 Stratigraphy

Four fluvial sections from the Pentiction Group (Glenrosa and White Lake Road Sections), Princeton Group (Hardwick Sandstone Section), and Kamloops Group (McAbee Section) were measured and described in detail. These sections were chosen based on the lack of previously published stratigraphy, abundance of possible ignimbrites for stable isotope analyses, and the abundance of imbricated clasts and cross-stratified strata for paleocurrent analyses. The White Lake Road, Hardwick Sandstone, and McAbee Sections were described at the decimeter scale. The Glenrosa Section was measured on a 0.5 m scale. Locations of stratigraphic sections are presented in Figure 4.1 and the generalized correlated stratigraphic sections are presented in Figure 4.2. Figure 4.3 shows photos from each stratigraphic section. Appendix 1 contains detailed stratigraphy at each location.

3.2 Volcanic Glass Stable Isotope Analyses

The dominant control on the stable isotope ratios of precipitation in mountainous regions is the progressive depletion of deuterium from the vapor phase due to adiabatic cooling of air masses as they rise over topography (Dansgaard, 1964; Poage and Chamberlain, 2001). After deposition, volcanic glass hydrates with meteoric waters within less than 10,000 years (Friedman et al., 1993; Cassel and Breecker, 2017). Meteoric water hydrates volcanic glasses through diffusive hydration, interdiffusion of hydrogen and soluble cations, and hydrolysis (e.g., Cerling et al., 1985; Bunker, 1994). Thus δD_{glass} values of volcanic glass samples can be used as a proxy for the δD value of local meteoric water shortly after the time of deposition. Local meteoric water δD values represent the hypsometric mean of precipitation δD values within the drainage basin above the sample location (Rowley, 2001), so the difference between δD values at the top and the bottom of a drainage basin is a minimum estimate of the difference in precipitation δD values across a drainage.

Tuff and ignimbrite samples were prepared following the methods of Cassel and Breecker (2017). Samples were crushed with a ceramic mortar and pestle, then sieved to the 70 – 150 μm size fraction. Samples were rinsed twice with 10% hydrochloric acid for 45 seconds to remove carbonates, followed by two 30 second rinses with 8% hydrofluoric acid

(HF) to remove clays and iron oxides adhered to the exterior of the volcanic glass samples. If clay minerals were present on the glass shard surfaces, one additional rinse of 8% HF was utilized. Samples were then run through a Frantz isodynamic magnetic separator to remove biotite, magnetite, and other magnetic minerals. Heavy liquid separations with lithium metatungstate, gradually lowered from a starting density of 2.7 kg/L, removed quartz and feldspars from the sample. Heavy liquid separation was repeated until volcanic glass fractions reach 95% purity. The degree of alteration and purity of the volcanic glass fractions were checked with a petrographic microscope. Only samples with no visible feldspar or biotite, coherent glass shard structure, and minimal visible alteration were analyzed, minimizing the potential of analyzing original magmatic or more recent waters incorporated during destruction of the volcanic glass structure. This treatment has little effect on volcanic glass chemistry (e.g., Cerling et al., 1985; Sarna-Wojcicki and Davis, 1991; Cassel et al., 2012; Cassel and Breecker, 2017).

Hydrogen isotope ratios of hydrated volcanic glasses were measured at the University of Texas at Austin with a Thermo Scientific TC-EA coupled with a Thermo Scientific MAT 253 gas source isotope ratio mass spectrometer. Three aliquots per sample were isotopically analyzed for consistency and error analysis. Four internationally certified standards and one in-house volcanic glass standard were run with each sample to correct for mass bias and drift of the combustion reactor. Analysis of the certified standards were repeated throughout the run and produced the following mean values: IAEA-C3 cellulose, $\delta D = -33.0\text{‰}$; IAEA-CH-7 polyethylene foil, $\delta D = -103.3\text{‰}$; IAEA-22 oil, $\delta D = -118.6\text{‰}$; and NBS-30 biotite, $\delta D = -76.1\text{‰}$. Volcanic glass reference material 057SH produced a δD value of $-149.8 \pm 3.1\text{‰}$ and a mean water content of 2.95%. Water contents were calculated as a measure of total H in the Isodat software. All hydrogen isotope ratios are reported relative to the standard mean ocean water (SMOW).

3.3 Paleoaltimetry Model

A Rayleigh distillation and air mass lifting model was used to determine the isotopic lapse rates and to calculate the paleoelevations from δD_{glass} values of ignimbrite and tuff samples (Cassel et al., 2014; Rowley et al., 2001). This model considers condensation and precipitation of an air mass as it rises and cools adiabatically due to a barrier and calculates

the resulting change in δD values. Additionally, the temperature dependent equilibrium fractionations between vapor and liquid and vapor and ice due to the air mass rising and cooling are considered with this model (Rowley et al., 2001). The model also considers a range of altitudes ($1,500 \pm 500$ m) and the subsequent weighted average of isotopic concentrations above the surface (Rowley et al., 2001). The model considers a single source of initial vapor, but changes in the isotopic concentration of this source are considered by using low elevation sites (Cassel et al., 2014). This model is calibrated to a modern isotopic lapse rate from measured meteoric surface and precipitation waters from the Coast Range near the latitude of Vancouver (Yonge et al., 1989).

3.4 Trace and Rare Earth Elemental Analyses

Tephrochronology is an important method for locally and regionally correlating tephra deposits to constrain paleoclimatic and paleogeographic trends within terrestrial and marine stratigraphic sections (Lowe, 2011). Tephrochronology studies include detailed physical and mineralogical descriptions, geochemical analyses of glass shards and minerals including major, minor, and trace element concentrations, and high-resolution geochronology (Lowe, 2011). These analyses permit direct comparisons of stratigraphy and glass geochemistry to the global paleoclimatic record and provide a geochronologic framework for robust interpretations of basin hydrology and connectivity, regional climate controls, and paleotopography.

Twelve volcanic glass samples were analyzed by solution ICP-MS at the Washington State University Peter Hooper GeoAnalytical Laboratory. 2 mg of powdered glass was fusion-dissolved with di-lithium tetraborate, followed by open-vial mixed acid digestion with hydrofluoric acid. Measurement of 14 rare earth elements and 13 additional trace elements was completed on an Agilent model 4500 ICP-MS. Three in-house rock standards were used per batch of 18 unknowns to accomplish standardization. Concentrations and drift corrections are calculated offline. Precision for this method is 5% for the REEs and 10% for trace elements.

3.5 U/Pb Geochronology

Nine ignimbrite samples were crushed and sieved between 70 μm and 250 μm . Repeated passes through a Frantz isodynamic magnetic separator removed biotite, magnetite, and other magnetic minerals. Density separation using a Methylene Iodine (CH_2I_2) heavy liquid solution set at 3.3 kg/L removed lower density minerals including quartz, feldspar, and apatite. Individual zircon grains were then handpicked, epoxy mounted, and polished. Cathodoluminescence (CL) imaging of the internal structures of all zircon grains were obtained at the University of Idaho SEM Laboratory. Isotope ratios were measured via laser ablation inductively-coupled plasma mass spectrometry (LA-ICPMS) using a New Wave UP-213 laser coupled to a Finnigan Element2 mass spectrometer at the Peter Hooper GeoAnalytical Laboratory. Backgrounds were measured followed by unknown grain measurements of masses 204, 206, 207, 208, 232, and 238 with a spot diameter of 30 μm . The reference material Plesovice was used as the external standard for U/Pb ratios. High precision dating of Plesovice by ID-TIMS yields a U/Pb age of 337.13 ± 0.37 Ma (Slama et al., 2008). Data was corrected for time-dependent fractionation of $^{206}\text{Pb}/^{238}\text{U}$ with a regression to $t=0$. Time-independent fractionation was corrected by normalizing U/Pb and Pb/Pb ratios to standard analyses. $^{238}\text{U}/^{206}\text{Pb}$ ages were plotted on Tera-Wasserburg plots anchored with a common lead composition to identify U/Pb ages influenced by common lead. Weighted mean ages were calculated with concordant $^{238}\text{U}/^{206}\text{Pb}$ ages using Isoplot 4.1 (Ludwig, 1999). Error was calculated by combining the systematic and analytical uncertainties in quadrature and never exceeds 2%.

4.0 Results

4.1 Stratigraphic Characteristics

The sequence stratigraphy is characterized by four dominant depositional styles with distinct grain sizes, sorting, sedimentary structures, and bed geometry. Figure 4.2 and Figure 4.3 shows the generalized stratigraphic sequence in the region and characteristic photos from each stratigraphic section, respectively. These features provide evidence for interpretations of depositional environments and correlations of the ages and locations of the sediments.

Lithofacies characterizations are based on diagnostic criteria from Miall (1996).

4.1.1 Princeton Group – Allenby Formation – Hardwick Sandstone

The Hardwick Sandstone Unit is a 30 m thick section which forms the basal conglomerate and sandstone of the Allenby Formation (Fig. 4.1). The outcrop is north of Princeton on the east side of Highway 5a, north of Summer's Creek (Fig. 4.3). Strata are split into three distinct lithofacies (Table 4.1). Lithofacies PC1 consists of 0.25-3 m thick, irregularly bounded beds of clast-supported, poorly sorted, sub-rounded to well-rounded, pebble to boulder conglomerate with weak imbrication and no grading. Lithofacies PC1 contains heavily weathered granite, lightly weathered granite, lesser basalt and gabbro, and rare tuff clasts with a very coarse-grained, angular to sub angular, poorly sorted matrix. Lithofacies PC2 consists of 0.25-1 m thick, laterally discontinuous, irregularly bounded beds of clast-supported, moderately sorted, sub-rounded to well-rounded, pebble to cobble conglomerate with strong imbrication and weak to no grading within beds. Strata of Lithofacies PC2 range from 0.25 to 3 m in thickness. Lithofacies PC2 clast compositions are dominated by granites, basalts, and gabbros with a medium- to very coarse-grained, sub-angular to sub-rounded, moderately sorted matrix. Numerous concave up bounded, moderately sorted, sub-rounded, medium- to coarse-grained sandstone lenses and minor clay and siltstone lenses are present in Lithofacies PC2. Lithofacies PC3 consists of laterally discontinuous, irregular-bounded beds of sub-angular to sub-rounded, moderately sorted sands with weak normal grading within beds. Strata of Lithofacies PC3 range in thickness between 0.25 to 3 m. Lithofacies PC4 consists of 0.1-0.25 m thick, laterally discontinuous, irregularly-bounded beds of moderately to well-sorted, sub-rounded, medium- to coarse-grained, normal graded sandstones with 1 mm thick silt and tuff beds. Strata of Lithofacies

PC4 are up to 0.5 m thick. Lithofacies PC5 consists of 0.1 m laterally discontinuous beds of well sorted, sub-rounded to well-rounded, planar laminated, fine- to medium-grained sands.

Table 4.1. Hardwick Sandstone Unit Lithofacies Descriptions and Depositional Environments

ID	Composition	Sedimentary Features	Corresponding Depositional Environment
PC1	Clast-supported gravel	Weak imbrication no grading	Longitudinal bedforms (high flow regime)
PC2	Clast-supported gravel	Strong imbrication, weak grading in sand lenses	Longitudinal bedforms with scour fills
PC3	Sand, fine to medium	Broad, shallow scours, graded bedding	Scour fills in channel
PC4	Sand, medium to coarse	Graded beds with mm silt and ash interbeds	Scour fills in channel (low flow)
PC5	Sand, fine to medium	Planar laminations	Plane-bed flow

4.1.2 Kamloops Group – Tranquille Formation – McAbee Beds

The McAbee beds located between Kamloops and Cache Creek (Fig. 4.1) consist of abundant ash-fall tuffs interbedded with silts, sands, and conglomerates. Previous studies focused on the abundance of well-preserved fossil biota and provided insight into the Eocene climate in southern British Columbia (e.g., Hills, 1965; Wilson, 1980; Archibald et al., 2010, Greenwood and Wing, 1995; Smith et al., 2010). But detailed stratigraphy of the McAbee beds has yet to be described. There are three distinct lithofacies from 30 m of stratigraphy at the McAbee beds (Fig. 4.2) (Table 4.2). Lithofacies MB1 comprises 3-4 m of laterally discontinuous, irregularly-bounded beds of clast-supported, poorly sorted, pebble to boulder, conglomerate with well-rounded to subrounded clasts of andesites and ignimbrites with a tuffaceous sandy matrix. Lithofacies MB1 contains multiple concave up lenses of 0.5-1 m thick, imbricated, moderately sorted, pebble to cobble conglomerate with a sandy matrix. Lithofacies MB2 consists of 1-10 cm beds of fine- to coarse-grained, tuffaceous sandstones with normal grading, soft sedimentary deformation, and abundant 0.2-10 cm air-fall tuff beds. MB2 contains minor fossiliferous mudstone to siltstone interbeds. Lithofacies MB3 consists of mm to cm beds of volcanoclastic, red to gray, fossiliferous, organic-rich, microlaminated clays and thinly bedded organic-rich to organic-poor siltstones. Lithofacies MB3 contains abundant 1-4 cm, fine-grained air-fall tuff beds. The strata of Lithofacies MB3

range between 0.25 to 7 m. Lithofacies MB3 contains woody debris, lobed leaves, metasequoia fossils and minor burrows and mud cracks on the bedding planes.

Table 4.2. McAbee Beds Lithofacies Descriptions and Depositional Environments

ID	Composition	Sedimentary Features	Corresponding Depositional Environment
MB1	Clast-supported gravel	Imbrication with weak grading and gravel lenses	Longitudinal bedforms with scour fills
MB2	Sand, fine to coarse	Graded beds with soft sedimentary deformation	Fluvial-Lacustrine (high inflow)
MB3	Organic-rich to organic- poor mud to silt	Weak or no grading and fine lamination	Fluvial-lacustrine

4.1.3 Penticton Group – White Lake Formation

The 1.1 km thick White Lake Formation unconformably overlies the Marron and Marama Formations and unconformably underlies the volcanoclastic strata of the Skaha Formation (Fig. 4.1) (Church, 1973; McClaughry and Gaylord, 2005). There are ten lithofacies from two well-preserved stratigraphic sections near Penticton (Table 4.3) (Fig. 4.2). The first stratigraphic section (~230 m), referred here after as the White Lake Road section, is located to the southwest of Penticton along White Lake Road and was partially described by McClaughry and Gaylord (2005). The second stratigraphic section (218 m), referred here after as the Glenrosa Section, is located north of Penticton at the Glenrosa Exit (Fig. 4.3).

The gravel lithofacies (WL1, WL2, and WL3) within the White Lake Formation are present in both the Glenrosa and White Lake Road Sections, but these lithofacies are dominate in the Glenrosa section. Lithofacies WL1 consists of 0.25 to 9 m, discontinuous, irregularly-bounded beds of clast-supported, poorly sorted, well-rounded, pebble to boulder, volcanoclastic conglomerate with weak imbrication and weak normal grading within beds. Lithofacies WL1 contains dominantly pebble to boulder, andesite and ignimbrite clasts with abundant woody debris and minor pebble to cobble sandstone clasts. Lithofacies WL2 consists of 0.5 to 10 m, discontinuous beds of irregularly-bounded, clast-supported, poorly sorted, sub-angular to subrounded, granular to boulder, weakly imbricated volcanoclastic conglomerate with laterally discontinuous, normal graded, volcanoclastic sandstone lenses.

Lithofacies WL3 consists of 0.1 to 9 m, discontinuous, irregularly-bounded beds of matrix-supported poorly sorted, sub-angular to subrounded, granular to boulder, volcanoclastic conglomerate with weak to no grading within beds. Lithofacies WL3 contains dominantly granular to boulder tuffaceous clasts with abundant woody debris and minor granular coal and lithic clasts.

Table 4.3. White Lake Formation Lithofacies Descriptions and Depositional Environments

ID	Composition	Sedimentary Features	Corresponding Depositional Environment
WL1	Clast-supported gravel	Weak imbrication, graded bedding	Longitudinal bedforms (high flow regime)
WL2	Clast-supported gravel with sand	Weak grading in sand lenses, weak imbrication	Longitudinal bedforms with scour fills
WL3	Matrix-supported gravel	Weak or no grading	Plastic debris flow
WL4	Sand, fine to very coarse	Solitary or grouped trough cross-beds	Sinuuous-crested and linguoid dunes in channel
WL5	Sand, very fine to coarse	Broad, shallow scours, graded bedding	Scour fills in channel
WL6	Sand, very fine to coarse	Solitary ripple forms with mud drapes, cross lamination	Ripples (lower flow regime)
WL7	Organic-rich sand, very fine to medium	Fine Lamination	Overbank or waning flood deposits
WL8	Mud to silt	Fine Laminations	Overbank, abandoned channel, or waning flood deposits
WL9	Organic-rich mud to silt	Fine Lamination of organic-rich material, soft sedimentary deformation	Backswamp or abandoned channel deposits
WL10	Coal	Bedding thickness ranges from 0.1 to 2 meters	Vegetated swamp deposits

The sand lithofacies (WL4, WL5, and WL6) are present in both the Glenrosa and White Lake Road Sections, but these lithofacies are more dominate in the White Lake Road Section. Lithofacies WL4 consists of 0.25 to 1.5 m laterally discontinuous, planar- and irregularly-bounded beds of moderately sorted, sub-angular to subrounded, fine- to very coarse-grained, volcanoclastic sandstone with solitary or group trough cross-beds and

abundant woody debris and metasequoia fossils. Some beds contain minor pebble clasts. The strata of Lithofacies WL4 reach a maximum thickness of 8 m. Lithofacies WL5 consists of 0.25 to 1.25 m laterally discontinuous, planar- and irregularly-bounded beds of moderate to well sorted, sub-angular to subrounded, very fine- to very coarse-grained, volcanoclastic sandstone with broad, shallow scours, normal graded beds, abundant woody debris and metasequoia fossils. Strata of Lithofacies WL5 reach a maximum thickness of 2.5 m. Lithofacies WL6 consists of 0.1 to 0.25 m, laterally discontinuous, planar- and irregularly-bounded beds of well sorted, subrounded, very fine- to coarse-grained, volcanoclastic sandstone with solitary ripple forms with mud drapes and abundant cross lamination and woody debris.

The clay, silt, and coal lithofacies (WL7, WL8, WL9, and WL10) are present in both the Glenrosa and White Lake Road Sections, but these lithofacies are more dominate in the White Lake Road Section. Lithofacies WL7 consists of 0.1-.25 m, planar-bounded, broad sheet-like, beds of organic-rich, well sorted, subrounded to rounded, very fine- to medium-grained, volcanoclastic sandstone with abundant woody debris and minor pebble lag on bedding surfaces. The strata of Lithofacies WL7 reach a maximum thickness of 0.5 m. Lithofacies WL8 consists of 0.05-0.1 m, planar-bounded, broad sheet-like, beds of interbedded organic-poor, laminated mudstones and thinly bedded volcanoclastic siltstones with abundant woody debris. Strata of Lithofacies WL8 reach a maximum thickness of 3 m. Lithofacies WL9 consists of 0.01-0.05 m thick beds of interbedded organic-rich, laminated mudstones and thinly bedded volcanoclastic siltstones with abundant soft sedimentary deformation and woody debris. Strata of Lithofacies WL9 reach a maximum thickness of 1.75 m. Lithofacies WL10 consists of 0.1-2 m planar-bounded, broad sheet-like, coal beds.

4.2 Field Occurrences and Sample Descriptions of Ignimbrites and tuffs

Rhyolitic to andesitic ignimbrite and tuff deposits are abundant in the Eocene basins of southern British Columbia and northern Washington. Ignimbrite and tuff deposits are found interbedded within fluvial and lacustrine strata and unconformably overlying older volcanic and pre-volcanic rocks. The ignimbrites are laterally discontinuous, vitric, massive to bedded, poorly sorted, and routinely contain medium- to very coarse-grained lithics, woody debris, white or yellow pumice, and abundant ash. Volcanic glasses within ignimbrite

deposits are locally altered; the units contain both zeolitized and clay mineralized zones. The degree of welding varies between individual ignimbrites from unwelded to densely welded. ~130 ignimbrite samples were collected from the region, twelve of which contained unaltered volcanic glass for TREE analyses and δD_{glass} analyses. Nine of these samples contained enough large, euhedral zircons for U/Pb radiometric dating.

In the Princeton Group, five ignimbrite samples were collected and analyzed from four different units within the Allenby Formation. Paleocurrent measurements of the imbricated clasts within the Hardwick Sandstone Unit yielded an easterly flow from the Princeton area indicating an Eocene catchment basin likely contained the Coast and Intermontane belts. The stratigraphically oldest sample, 63PC, was collected from a finely bedded, tuffaceous sandstone from the Summers Creek Sandstone Unit. Samples 17PC and 18PC were collected from the overlying Asp Creek Ash Unit consisting of interbedded tuffaceous sandstones, minor siltstones, and zeolitized rhyolite tuffs. Sample 17PC was collected from a ~30 cm, fine-grained, tuffaceous, sandstone bed. Sample 18PC, stratigraphically overlying sample 17PC, was collected from a ~10 cm coarse-grained tuffaceous sandstone bed. Sample 64PC, was collected from the overlying Tailings Ash Unit consisting of bedded, rhyolite tuff with local zeolite zones and minor tuffaceous sandstones. Sample 67PC(A), collected from the overlying ~23 m thick Bromley Vale Tephra Unit consisting of zeolitized rhyolite breccias and tuffs with abundant plant debris and lithic clasts.

In the Kamloops Group, five ignimbrite samples were collected and analyzed from the famous fossil locality known as the McAbee beds. The McAbee beds, located on the western edge of the Kamloops Group include clast-supported pebble to cobble volcanoclastic conglomerates, organic-rich, finely laminated claystones to sandstones, with interbedded volcanic tuffs representing episodic distal volcanic ash deposition in a fluvial-lacustrine setting. Previous researchers concluded fluvial input flowed dominantly from the eastern Omineca Belt and the Intermontane Belt (Tribe, 2005). From oldest to youngest, samples 033MB(A), 34MB(A), 35MB(D), 39MB, and 42MB were collected from 2-6 cm air-fall tuff beds interbedded with the claystones and sandstones. Sample 30FK was collected from a fine-grained tuffaceous sandstone of the Shorts Creek Formation located on the eastern side

of the Kamloops Group. Sample 73CV was collected from a medium-grained bedded ignimbrite from the Kamloops Group east of the Okanagan Valley in the Omineca Belt.

4.3 Geochemical Correlation of Ignimbrites

TREE concentrations are normalized to chondrite values from Sun and McDonough (1989). Appendices 2 and 3 contain full TREE results and volcanic glass petrographic images, respectively. Normalized TREE concentrations are plotted against previous bulk rock TREE analyses of andesites, basalts, and rhyolites from the Republic Group, Princeton Group, Kamloops Group, and Goosly Volcanics (Fig. 4.4; Morris et al., 1999; Ickert et al., 2007; Breitsprecher, 2003; Dostal, 2001). Volcanic glass samples are split into three distinct groups based on the ratios of La/Yb, a measurement of the enrichment of light REE (LREE) relative to the heavy REE (HREE), and Eu/Eu*, a measurement of the magnitude and direction of the Eu anomaly.

Group #1 includes samples 30FK, 17PC, 34MB(A), 35MB, 63PC, and 73CV and shows similar TREE trends to previously reported regional bulk rock geochemistry including the enrichment of LREE relative to HREE (La/Yb= 14.11 – 52.55) and a minimal Eu anomaly (Eu/Eu*= 0.73 – 1.22) (Fig. 4.4). Within Group #1, Sample 73CV yields an elevated Th/Hf ratio and the enrichment of the immobile and incompatible elements Th and Zr, indicating a distinct ignimbrite unit (Fig. 4.4). Sample 30FK has low Th, Hf, and Zr concentrations and shows a relatively small negative Eu anomaly (Eu/Eu*= 0.73), indicating a distinct ignimbrite unit. Samples 34MB(A) and 63PC have similar spider diagram profiles, but Sample 34MB(A) is more enriched in the incompatible and immobile high field strength elements Hf and Zr, likely indicating two distinct ignimbrite units or two distinct eruptions from the same source. Samples 35MB and 17PC show similar REE profiles with enriched LREE relative to the HREE (La/Yb=25.17 and 26.91, respectively), but Sample 35MB is more enriched in Hf and Zr values indicating a chemically distinct ignimbrite unit or a later eruption from the source of 17PC (Fig. 4.4).

Samples 33MB(A), 39MB, and 18PC comprise the second chemically distinct group of samples and show a similar trend of enriched LREE relative to the HREE (La/Yb= 1.80 – 9.14) as the regional bulk rocks. This group's positive Eu anomaly (Eu/Eu*= 2.11 – 6.28) contrasts with the regional bulk rock geochemical trend. Sample 18PC has similar Ce and Rb values to 33MB(A), but it has lower immobile and incompatible element concentrations (Hf

and Th) indicating a distinct ignimbrite unit or an earlier eruption than Sample 33MB(A) and the stratigraphically younger Sample 39MB.

The third distinct geochemical group of samples includes 64PC and 67PC(A). Both samples show a lesser enrichment of the LREE relative to the HREE ($\text{La/Yb} = 2.20 - 3.42$) than the other volcanic glass samples and a large negative Eu anomaly ($\text{Eu/Eu}^* = 0.03 - 0.13$). Sample 64PC is enriched relative to Sample 67PC(A) in the incompatible and immobile elements Hf and Zr indicating two chemically distinct ignimbrite units or that 64PC represents a later eruption from the same source.

4.4 U/Pb Radiometric Dating

Nine new U/Pb radiometric dates of zircon grains from our sampled ignimbrites were determined to provide greater dating accuracy and precision of the stable isotope samples (Table 4.4; Fig. 4.5). Appendices 4 and 5 provide the full U/Pb zircon analyses and the CL images. All ages are reported as $^{238}\text{U}/^{206}\text{Pb}$ weighted means with 2σ uncertainty. The accuracy of U/Pb dating of zircon with LA-ICP-MS is $\pm 2\%$, based on the accuracy of the zircon standard Plesovice (Slama et al., 2008). The analyses yielded two distinct age populations within the Princeton Group and one distinct age population at the McAbee beds within the Kamloops Group.

In the Princeton Group, the stratigraphically oldest sample 63PC from the Summers Creek Sandstone Unit yielded 17 concordant dates with a U/Pb weighted mean of 50.01 ± 0.41 Ma (MSWD=1.6). Previous K/Ar-biotite dating placed the maximum depositional age at 46.2 ± 2 Ma (Read, 2000). Samples 18PC, 64PC, and 67PC(A) from the stratigraphically younger Asp Creek Ash Unit, Bromley Vale Tephra Unit, and Tailings Ash Unit, respectively, yielded weighted mean dates between $48.23 - 47.33$ Ma ± 0.26 Ma (MSWD = 1.3). These are the first dates from these units.

In the McAbee beds of the Kamloops Group, the stratigraphically oldest sample yielded 17 concordant dates with a U/Pb weighted mean of 51.00 ± 0.31 Ma (MSWD = 1.09). The stratigraphically youngest sample yielded 16 concordant dates with a U/Pb weighted mean of 50.80 ± 0.34 Ma (MSWD = 1.4). These new dates agree with previous K/Ar dating of sanidine and biotite from volcanic ash layers within the McAbee beds that

range from 52 to 49 ± 2 Ma (Hills and Baadsgaard, 1967), but provide much greater precision (Fig. 4.6).

Three samples from Republic, Falkland, and Creighton Valley yielded fewer zircon grains for analyses, but these dates still provide improved precision relative to previous K/Ar age assignments. Within the Republic Group, sample 43RP from the Sanpoil Formation yielded 12 concordant dates with a U/Pb weighted mean of 52.43 ± 0.55 Ma (MSWD = 2.7). This date determination agrees with previous K/Ar dates from plagioclase, hornblende, and biotite, which range from 53.4 ± 2.0 Ma to 48.4 ± 3.0 Ma (Pearson and Obradovich, 1977), but provide much greater precision. Within the Kamloops Group, sample 30FK from the Shorts Creek Formation yielded nine concordant dates with a weighted mean age of 50.2 ± 1.0 Ma (MSWD = 2.7). This date agrees with previous whole rock K/Ar radiometric dating that constrained the Shorts Creek Formation at 50.5 ± 1.8 Ma (Ewing, 1981). Sample 73CV from Creighton Valley yielded six concordant dates with a weighted mean age of 50.14 ± 0.91 Ma (MSWD = 2.4) (Fig. 4.5). This is the first age from this unit.

Table 4.4. U/Pb Age Determinations of Zircons

Sample ID	Latitude (°N)	Longitude (°W)	U/Pb Weighted Mean (Ma) (<i>n</i>)	MSWD
43RP	48.615	118.733	52.43 ± 0.55 Ma (12)	1.60
34MB(A)	50.797	121.142	51.00 ± 0.31 Ma (17)	1.09
39MB	50.797	121.142	50.80 ± 0.34 Ma (16)	1.40
30FK	50.515	119.632	50.20 ± 1.00 Ma (9)	2.70
73CV	50.148	118.851	50.14 ± 0.91 Ma (6)	2.40
63PC	49.563	120.511	50.01 ± 0.41 Ma (18)	1.60
67PC(A)	49.423	120.596	48.23 ± 0.26 Ma (19)	1.30
18PC	49.464	120.512	48.18 ± 0.35 Ma (17)	1.20
64PC	49.426	120.554	47.33 ± 0.24 Ma (18)	1.18

4.5 δD_{glass} Analytical Results and Paleoaltimetry Model

Measured δD_{glass} values from southern British Columbia range from -82‰ to -190‰ (Table 4.5; Fig. 4.6). Two samples have significantly lower δD_{glass} values than those from partially zeolitized, thus likely evaporative lacustrine, tuff samples. Sample 64PC, from the Tailings Ash Formation within the Princeton Group, has a δD_{glass} value of $186.5 \pm 2.0\text{‰}$, and Sample 30FK, from the Shorts Creek Formation from the eastern edge of the Kamloops

Group, has a δD_{glass} value of $-197.3 \pm 2.5\text{‰}$. Paleocurrent measurements from imbricated conglomerates of the Princeton Group indicate Eocene meteoric waters were sourced from the Coast and Intermontane Belts (Fig. 4.1). Previous researchers concluded an eastern source of Eocene meteoric waters for the Kamloops Group including the eastern Omineca Belt and the Intermontane Belt (Tribe, 2005).

Table 4.5. Measured δD_{glass} Values

Sample ID	Latitude (°N)	Longitude (°W)	Modern Elevation (m)	Distance from Modern Shoreline (km)	Measured δD_{glass} (‰) V-SMOW	2 σ Error (‰)	Average Water Content (%)	2 σ Error (%)
17PC*	49.464	120.512	650	181	-134.1	1.4	3.0	0.1
18PC	49.464	120.512	650	181	-93.3	0.9	8.1	0.1
63PC	49.563	120.511	770	180	-91.7	5.1	4.1	0.3
64PC	49.426	120.554	834	183	-186.5	1.9	4.9	0.1
67PC (A)	49.423	120.596	940	183	-98.6	9.7	9.5	0.5
33MB(A)	50.797	121.142	609	225	-109.4	2.2	9.6	0.1
34MB(A)	50.797	121.142	610	225	-111.7	3.2	8.5	0.4
35MB(D)	50.797	121.142	611	225	-112.6	6.5	4.3	0.3
39MB	50.797	121.142	613	225	-114.6	2.3	10.2	0.3
42MB	50.797	121.145	615	225	-114.7	1.1	8.1	0.1
73CV	50.148	118.851	1387	325	-76.2	4.7	1.7	0.3
30FK	50.515	119.632	1044	306	-197.3	2.5	2.6	0.1

* Sample 17PC was partially altered and recrystallized, as visible under cross-polarized light, so this δD_{glass} value reflects modern meteoric waters, therefore we did not consider the sample in this study.

Five samples from the McAbee beds show a decrease in δD_{glass} values with movement up section from -109‰ to -115‰ ($\pm 3.5\text{‰}$ for all but one sample). Princeton Basin sample values indicate hydration from two different source waters. Sample 63PC, taken from a reworked ignimbrite deposited in a lake, yielded a measured δD_{glass} value of $-88.1\text{‰} \pm 2.0\text{‰}$, possibly indicating an evaporative (enriched) signature. Sample 18PC, from the lacustrine-deposited Asp Creek Ash unit, yielded a measured δD_{glass} value of $-93.3\text{‰} \pm 2\text{‰}$. Sample 67PC(A) from the younger lacustrine-deposited and partially zeolitized Bromely Vale Ash Unit yielded a measured δD_{glass} value of $-98.6\text{‰} \pm 9.7\text{‰}$. When altered, volcanic glass in ash beds within fluctuating-profunda strata are typically altered to zeolite minerals, suggesting that lake waters were often alkaline during evaporative periods (Goodwin and Surdam, 1967). Petrographic analysis of sample 17PC shows the breakdown

of glass shard structure and crystallization of clay minerals. That sample recorded a δD_{glass} value of $-134.1\text{‰} \pm 2.0\text{‰}$. The modern δD_{water} concentration of creek water near the location of sample 17PC is $-126 \pm 2.0\text{‰}$ (Appendix 2) (Yonge et al., 1989). It is likely sample 17PC is reflecting more recent hydration of clay minerals by meteoric waters and not paleometeoric water in glass, therefore, we did not use this sample in elevation calculations.

5.0 Discussion

5.1 Stratigraphic Interpretations

5.1.1 Princeton Group – Allenby Formation – Hardwick Sandstone

Lithofacies PC1 of the Hardwick Sandstone Unit represents deposition of clast-rich debris flows with minimal fluvial influence. The mix of heavily to lightly weathered granitic clasts suggests material was sourced from proximal pre-Eocene sedimentary and igneous rocks. The irregularly bounded, laterally discontinuous sands of PC2 were deposited as shallow fluvial scour fills. The longitudinal gravel bedforms of Lithofacies PC3, with numerous concave up sandy lenses, indicate intermittent scouring and infilling by small fluvial channels. Reconstructed paleocurrent measurements suggests paleoflow from west to east. Lithofacies PC3 and PC4 are interbedded indicating periods of erosive channel development and bedform migration. Multiple channel scours are present laterally adjacent within one bed, indicating multiple active channels. The small gravel conglomerate and sandstone lenses of PC4 become more dominant towards the top of the stratigraphic section. The fine planar laminated sands of PC5 indicate the system was periodically in lower stage flow. The development of multiple small channels, abundant imbricated conglomerate beds, trough and planar stratified sands, and air-fall ash deposition is indicative of a shallow, braided fluvial facies association model with minor distal volcanic input (PC-MA2). Minor debris flow deposits and predominance of local basement clasts indicates local channel relief.

5.1.2 Kamloops Group – Tranquille Formation – McAbee Beds

Here we present two lithofacies model associations (MB-MA1 and MB-MA2) of the McAbee beds stratigraphy. MB-MA1 includes Lithofacies MB1 and represents braided fluvial deposition with input from proximal volcanics. Braiding was likely a result of increased volcanic and volcanoclastic supply into the existing paleovalley. Scour fills of imbricated pebbles and cobbles indicate channel development and infilling during periods of decreased source availability. MB-MA2 includes Lithofacies MB2 and MB3 and represents episodic deposition of lacustrine strata, likely a result of episodic damming of a paleovalley. The abundance of thin fine-grained tuff beds is indicative of distal air-fall ashes during a regional magmatic event. The irregular presence of ostracods, fish, and other fossilized fauna suggest a fluctuating-profundal lake. This is supported by mud crack development near the

migrating shoreline during reduced volumes of inflow and continued evaporation or increased outflow. The coarse-grained, normal graded sandstones and prevalent soft sediment deformation of Lithofacies MB2 is indicative of periods of increased sediment supply and rapid deposition. Minor fossiliferous mudstone and siltstone interbeds represent periods of reduced fluvial input or deepening events. We interpret MB-MA2 as a fluctuating-profunda lake system, as defined by Carroll and Bohacs (1999), with syndepositional volcanism. In addition, the interbedded nature of the two lithofacies model associations is likely a result of episodic damming of the paleovalley with ignimbrites during periods of intense proximal volcanism, or shoreline and delta migration during fill cycles.

5.1.3 Penticton Group – White Lake Formation

The clast-supported, weakly imbricated conglomerates of Lithofacies WL1 and WL2 were likely deposited as longitudinal bedforms in high flow regimes. The sandy lenses within Lithofacies WL2 represents small scour fills and minimal channel development. Both lithofacies are dominated by tuff and andesite clasts, a result of proximal volcanism and abundant source availability. The matrix-supported conglomerates of Lithofacies WL3 represent gravity driven debris flows dominated by tuff and andesite clasts from proximal volcanism. The trough cross-bedded sands of Lithofacies WL4 represent sinuous-crested and linguoid dune development within fluvial channels. Lithofacies WL5 consists of shallow scours and graded bedding within the sands and represents scour infilling of fluvial channels. The solitary ripple forms with abundant mud drapes of Lithofacies WL6 represent ripple development with recurrent flow reduction allowing mud drape deposits on top of the ripple forms. Lithofacies WL7 includes finely laminated, organic-rich sands representing overbank or waning flood deposits. The finely laminated, organic-poor muds and silts of Lithofacies WL8 represent overbank, abandoned channel, and/or waning flow deposits. The finely laminated, organic-rich muds and silts of Lithofacies WL9 were deposited in a backswamp setting or in abandoned channels. The coal beds of Lithofacies WL10 represent vegetated swamp deposits adjacent to the active channel.

There are three facies model associations (WL-MA1, WL-MA2, and WL-MA3) from the White Lake Road and Glenrosa Sections. WL-MA1 consists of the lowest 60 m of the Glenrosa Section and is not present in the White Lake Road Section. It is dominated by thick

beds of matrix- and clast-supported conglomerates (WL1, WL2, WL3) with thin interbeds of sands and silts. Deposition of WL-MA1 likely occurred during high flow fluvial events with episodic gravity driven debris flows proximally sourced from adjacent high relief. Irregular scoured surfaces indicate prevalent episodic high flow erosional events followed by deposition of additional conglomerates and minor sands.

WL-MA2 consists of the lowest 40 m within the White Lake Road Section and the upper 160 m of the Glenrosa Section. It is dominated by conglomerate lithofacies (WL1, WL2, and WL3) with interbedded silts and sands. Deposition of WL-MA2 occurred during varied flow phases (high to low) with migrating channel bars, infilling of cross-stratified sands into scoured surfaces, and overbank deposition of silts and fine-grained sands during waning flooding events. Numerous matrix-supported conglomerates indicate episodic deposition of gravity driven debris flows sourced from adjacent high relief areas. The tuffaceous nature of the sands and gravels indicates a proximal source of the ignimbrites and volcanic flows. The deposition of the bottom of the White Lake Road Section and the top of the Glenrosa Section occurred in the same facies model association. But several differences exist between the two sections. First, the average grain size in the Glenrosa Section is coarser than the lower White Lake Section indicating a higher flow regime. In addition, fewer channel fills are identified in the Glenrosa Section indicating less mature channel and system development. The deposition of WL-MA2 occurred in a meandering fluvial setting with episodic volcanic debris flow deposition.

WL-MA3 consists of the upper 190 m of the White Lake Road Section and is dominated by sand lithofacies (WL4, WL5, WL6) with interbedded silts and clays. Deposition of WL-MA3 occurred during varied flow phases (high to low) with migrating channel bars, and numerous cross-stratified and normal graded sands. Scoured surfaces are present, but less abundant than in WL-MA2 indicating high flow erosional events are less common in WL-MA3. Overbank and vegetative swamp deposits are prevalent within WL-MA3 indicating episodic flooding events and full floodplain and back swamp development. The interbedded overbank and swamp deposition occurred often and suggests slow channel migration. The interbedded ignimbrite deposits suggest continued proximal deposition into the paleovalley. The deposition of WL-MA3 occurred in a meandering fluvial setting with abundant proximal and distal volcanic events recorded throughout.

The White Lake Road and Glenrosa Sections are at least partially correlative in time, contrary to previous interpretations by McClaughry and Gaylord (2005). We posit the two stratigraphic sections are representative of two stretches within the same fluvial system. The coarser, less mature lithofacies of the Glenrosa Section indicates source material is more proximal. This interpretation agrees with the southerly paleocurrent measurements taken in the White Lake Road Section. In addition, an ignimbrite deposited adjacent to the Glenrosa Section represents the likely source of the sediments. The lack of drastic lithofacies changes within the White Lake Formation indicates a short period of tectonic stability and fluvial development prior to rapid uplift and deposition of the alluvial volcanoclastic strata of the Skaha Formation.

5.2 Ignimbrite Geochemistry and Correlation

Compositions of twelve sampled ignimbrites range from andesite to rhyodacite. Except for two samples, geochemical trends are similar to the previously sampled bulk rocks including the enrichment of the LREE concentrations relative to the HREE concentrations ($La/Yb=3.16-26.91$), enrichment of the LILE concentrations, and the lack of a strong negative Eu anomaly (Fig. 4.4). The two youngest samples from the Princeton Group (67PC(A), 64PC) show the most evolved magmatic signatures, including a large negative Eu anomaly indicating plagioclase fractionation prior to the eruption. In addition, Sample 64PC plots near ocean island basalt compositions in almost all TREE diagrams indicating a highly primitive source. No ignimbrite samples from southern British Columbia can be confidently correlated based on their glass geochemistry. This is likely due to the multitude of Eocene source calderas and eruptive events. Deposition of the large ignimbrite units (10-20 m) occurred in local paleovalleys of restricted basins proximal to the source calderas. But the presence of the Princeton-type geochemistry in the air-fall tuffs from Kamloops Group suggests aerial transport of eruptive ash between the Princeton and Kamloops Basins.

Adakite signatures in regional volcanics have become an important line of evidence in determining the driving tectonic mechanism in the region. Adakites are intermediate to high-silica rocks with high Sr/Y and La/Yb ratios and low Y and Yb concentrations and are often associated with the partial melting of young garnet-bearing metabasalts in subduction settings (Defant and Drummond, 1990). The thermal trigger to create adakite signatures is

still debated. But asthenospheric upwelling due to slab rollback, slab windows, or slab detachment could provide a sufficient heat source to produce an adakitic signature (Bourdon et al., 2002; Thorkelson and Breitsprecher, 2005; Gao et al., 2007). In southern British Columbia, sixteen samples from the Princeton, Kamloops, and Penticton Groups show adakite signatures based on the criteria presented in Defant and Drummond (1990) (Breitsprecher et al, 2003; Ickert et al., 2007). A more precise adakite definition, however, produced by a review of all published adakite criteria, indicates only five of the previously reported sixteen samples are considered adakites (Castillo, 2012). All the newly redefined adakites are located within the Princeton Basin. The remaining eleven samples from the Kamloops, Penticton, and Princeton Groups are considered adakite-like and still suggest a primitive magmatic source. This study produced two samples (34MB(A) and 063PC) matching the adakite REE criteria. Volcanic glass samples from this study show increases in the Sr values with increased H₂O concentrations and suggest the highly mobile Sr signatures were possibly obtained during post-depositional meteoric alteration. We do not see similar correlations between other mobile elements and water content and suggest post depositional alteration had minimal to no effect on our REE concentrations, but we have eliminated Sample 34MB(A) as a possible adakite due to the importance of the Sr concentrations within the adakite criteria. In contrast, Sample 63PC shows an average wt. % water of only 4.1% and we consider this sample an adakite.

New ²³⁸U/²⁰⁶Pb zircon dates provide additional precision and accuracy to the maximum depositional ages of regional fluvial, lacustrine, and ignimbrite sedimentation. The oldest ignimbrite dated indicates the initiation of an ignimbrite flare-up event occurred in the Republic Graben at 52.43 ± 0.55 Ma. The new age of 50.01 ± 0.41 Ma from within the Princeton Basin suggests basin sediments are ~2-4 Ma older than previously reported (46.2 ± 2 Ma) (Hills and Baadsgaard, 1967). Based on total underlying strata, we suggest synchronous initiation of subsidence and accumulation in the Kamloops and Princeton Groups at ~52 Ma. The youngest ignimbrite sampled indicates the ignimbrite flare-up event continued to at least 47.33 ± 0.24 Ma. Based on stratigraphic correlations, sedimentation within the Princeton Basin likely continued through the middle Eocene.

Based on these ages, a regional ignimbrite flare-up event began in the Republic Graben at 52.43 ± 0.55 Ma and propagated northward into the Princeton and Kamloops

Basins by 51.00 ± 0.31 Ma. The ignimbrite flare-up event is likely directly related to the development and the propagation of a slab window developing under this region between ~ 56 and ~ 50 Ma. In addition, our new dates indicate deposition of the famous fossil localities including the McAbee beds, Falkland sediments, and early Princeton Group sediments, occurred during the EECO (52.6 – 50.3 Ma). Thus, these localities provide a mid-latitude terrestrial, fossil, and climatic record of high temperatures and high $p\text{CO}_2$ and can be directly compared to marine records and other terrestrial records from that climate event.

5.3 Hydrogen Isotope Ratios in Hydrated Volcanic Glass

New U/Pb dates indicate deposition of all the sampled ignimbrites and tuffs occurred within a 5 Ma interval. The near simultaneous hydration of volcanic glasses of these ignimbrites and tuffs and such a large range in measured $\delta\text{D}_{\text{glass}}$ values (-82‰ to -190‰) indicates the values represents local variations in depositional environment and hydrology, and not solely regional climatic or topographic changes.

In Princeton, the presence of local zeolite zones in all the ignimbrite and tuff units suggests fluctuating-profundal depositional environments where lake waters were often alkaline during evaporative intervals (Goodwin and Surdam, 1967). The evaporative periods drove the enrichment of deuterium within the lacustrine environments and hydrated volcanic glass with more enriched δD values. The Princeton Group samples 18PC, 63PC, and 67PC(A) were likely deposited in lacustrine environments and have more enriched δD values.

McAbee $\delta\text{D}_{\text{glass}}$ values range between -109.4 and -114.7‰ ($\pm 3.5\text{‰}$ for all but one sample). Our stratigraphic analysis of the McAbee beds indicates fluctuating profundal fluvial-lacustrine deposition (Carroll and Bohacs, 1999). The range of deuterium values likely reflects a slight evaporative trend within the paleolake. The increased depletion with movement upsection is likely a result of decreasing evaporation or a slight change in source waters of the paleolake. Only two samples, 64PC and 30FK, show no geochemical or physical indication of lacustrine influence on the $\delta\text{D}_{\text{glass}}$ concentration. Therefore, the $\delta\text{D}_{\text{glass}}$ values of these samples are the best proxy values for Eocene meteoric water and the basis for modeled paleoelevations.

Figure 5.1 shows our modeled isotopic lapse rate compared to modern surface water and precipitation data, modeled modern topography, and modeled Eocene topography. The model is most sensitive to changes in initial temperature (Cassel et al., 2014), paleoelevations were calculated assuming that air mass temperatures at 1500 m along the Eocene coast were 3-4°C higher than modern based on CLAMP-derived paleofloral analyses (Evans, 1991; Mustoe and Grannaway, 1997). Minimum and maximum paleoelevations were estimated assuming that initial air mass temperatures were no less than 3°C and no greater than 4°C higher than modern, respectively. The model validation predicts elevation profile from the modern Coast Range in southern British Columbia for all but three of the nineteen Coast Range samples (Fig. 5.1). For these initial conditions, the model predicts Eocene elevations of 2800-3000 ± 300 m from the Princeton and Falkland Basins. Increased $p\text{CO}_2$ in warm climates as posited in southern British Columbia could greatly reduce the isotopic lapse rate by up to ~8.1‰/km leading to the underestimation of modeled paleoelevations by 40% (Smith et al., 2010; Poulsen and Jeffery, 2011).

Precipitation isotope ratios often reflect air mass mixing, and atmospheric flow patterns can go around instead of over narrow topographic features (Galewsky, 2009). In contrast, the 1D model is limited to a singular air mass rising over topography. Precipitation in modern southern British Columbia, however, is dominantly sourced from the Pacific and the topography is consistent along strike for 1,500 km, so these model constraints are a close approximation to the modern. Further 3D modeling (e.g., Feng et al., 2014; Poulsen and Jeffery, 2011) is needed to address the possible roles of air mass mixing, high $p\text{CO}_2$, and evolving topography on precipitation δD and $\delta^{18}\text{O}$ values during the Eocene.

Our new model suggests previous paleoaltimetry estimates based on authigenic mineral proxies overestimated elevations in British Columbia due to their regional modeling approach versus our local modeling approach (Mulch et al., 2007; Mix et al., 2011). Our new calibrated hydrogen lapse rate of -3.5‰/100 m between 2,000 and 3,000 m from southern British Columbia is significantly higher than the previously modeled lapse rate (Fig. 5.1; Mulch et al., 2007; Mix et al., 2011). This likely due to the cooler initial air mass temperatures compared to the temperatures used to calibrate transects within the Sierra Nevada Mountains. Furthermore, paleoelevation estimates from paleofloral proxies,

paleophysiography and paleodrainage directions significantly underestimate paleoelevation by at least ~1 km.

5.4 Potential Tectonic Mechanisms

The data reported here yield new insights into the controls on the formation and evolution of the Eocene landscape and geology in southern British Columbia and northern Washington (Thorkelson and Taylor, 1989; Thorkelson, 1996; Haeussler et al., 2003; Ickert et al., 2007; Bao et al., 2014). Farallon slab rollback (e.g., Humphreys, 2009; Chamberlain et al., 2012; Smith et al., 2014) provides a unifying mechanism to account for the sweeping volcanism, core complex exhumation, and basin formation for the North American Cordillera from southern British Columbia to Nevada. This mechanism, however, does not fully account for the timing of volcanism and extension in the southern Canadian Cordillera. The new ignimbrites ages reported here support simultaneous initiation of regional basin subsidence and volcanism with no discernable north to south trend, with the exception of the early formation of the Republic Basin to the southern end of the study region – counter to the predicted movement of slab rollback. Future high-precision dating (TIMS or $^{40}\text{Ar}/^{39}\text{Ar}$) is necessary to test for this trend. Additionally, forearc volcanism remained active during proposed rollback, suggesting that a shallow slab may not have been present (Babcock et al., 1992). While there is a north to south trend in core complex ages from British Columbia to Nevada, there is not a local southward core complex trend within British Columbia and northern Washington, based on current thermochronologic data (Vanderhaeghe et al., 2002; Gordon et al., 2008; Cubley et al., 2013; Laberge and Pattison, 2007). Finally, there is not a regional trend of diagnostic basin characteristics, as has been proposed for rollback basins (Smith et al., 2014), including a progression from fluvial to lacustrine and finally volcanoclastic terrestrial lithofacies followed by an unconformity.

Bao et al. (2014) proposed a lithospheric delamination event commencing at ~55 Ma based on Rayleigh-wave tomographic and thermochronological data. But new ages and correlations reported here show no evidence of regional hinterland subsidence and accumulation prior to the regional ignimbrite flare-up, as is typical in delamination models (DeCelles et al., 2009). Our new paleoaltimetry results indicate high topography (2800-3000 ± 300 m) across the hinterland at the initiation of the ignimbrite flare-up event. This is in direct contrast with the delamination model as subsidence prior to delamination would

provide low elevations within the hinterland (DeCelles et al., 2009). Additionally, McClaughry and Gaylord (2005) and Read (2000) suggest the presence of basin bounding faults during the earliest basin accumulation, whereas basin bounding faults are typically absent from early subsidence during a delamination event (DeCelles et al., 2015). While lacustrine lithofacies are present throughout the region, they are not dominant in all basins, as suggested with delamination-linked basins, and notably absent in the White Lake Formation (McClaughry and Gaylord, 2005; DeCelles et al., 2015). Additionally, the positive anomaly in the Rayleigh-wave tomography data previously interpreted as a remnant block of delaminated lithosphere could also be related to edge-driven convection or the remnant Winona block associated with the subduction of the Juan de Fuca Plate (Bao et al., 2014; Hardebol et al., 2012; Mercier et al., 2009). Both interpretations fit within the slab window mechanism. The mantle lithosphere is thinned to modern levels in part by convective removal due to the upwelling asthenosphere through a slab window as seen in tomographic data of modern ridge subduction zones (Russo et al., 2010).

While diagnostic criteria for signatures of spreading ridge subduction and slab window propagation continue to be debated especially within the backarc (Thorkelson, 1996; Haeussler et al., 2003; Breitsprecher, 2003; Dostal et al., 2003; Sisson et al., 2003; Ickert et al., 2007), the formation of a slab window is our preferred mechanism driving the Eocene magmatic and basin evolution within the southern Canadian Cordillera. Initiation of the ignimbrite flare-up event and sedimentation started in the south within the Republic Graben at 52.43 ± 0.55 Ma. New ignimbrite ages show that volcanism began later to the north within the Kamloops and Princeton Groups, suggesting the initiation of a flare-up event and synvolcanic sedimentation began between 52 and 51 Ma. This is likely due to the northward propagation of the proposed slab window as modeled by Breitsprecher (2003). The initiation of core complex extension between 60-50 Ma corresponds directly to the timing of initial spreading ridge subduction (Vanderhaeghe et al., 2002), likely a result of the elimination of the boundary forces on the elevated Cordillera hinterland and heating of the mantle lithosphere due to asthenosphere upwelling through a slab window. And based on our revised distinctions, samples with adakite and adakite-like elemental signatures are constrained to basins along the strike of the proposed slab window at ~50 Ma (Breitsprecher, 2003), but true adakites are present only in the Princeton Basin.

6.0 Conclusions

1A. The White Lake Formation lithofacies model associations from the White Lake Road and the Glenrosa Sections include:

WL-MA1) The deposition of thick beds of matrix- and clast-supported conglomerates with thin interbeds of sands and silts occurred during high flow fluvial events with episodic gravity debris flows sourced from proximal volcanics. We interpret WL-MA1 as early deposition of a braided to meandering fluvial system.

WL-MA2) The deposition of moderately thick beds of matrix- and clast-supported conglomerates with interbedded silts and cross stratified sands occurred during varied flow phases (high to low) with migrating channel bars, infilling of cross-stratified sands into scoured surfaces, and overbank deposition of silts and fine-grained sands during flooding events. The deposition matrix-supported conglomerates occurred during episodic gravity debris flows. We interpret WL-MA2 as deposition of a meandering fluvial system.

WL-MA3) The deposition of the cross-stratified and normal graded sand lithofacies with abundant interbeds of silt, clay, and coal occurred during varied flow phases with migrating channel bars. Scoured surfaces are present, but less abundant than in WL-MA2 indicating high flow erosional events are less common in WL-MA3. Overbank and vegetative swamp deposits are prevalent indicating episodic flooding events and the development of full floodplains and back swamps. The interbedded overbank and swamp deposition suggests channel migration occurred slowly. We interpret WL-MA3 as deposition of a meandering fluvial system.

1B. The White Lake Road and Glenrosa Sections are correlative in time, contrary to previous interpretations, indicating the two sections are representative of two stretches of the same fluvial system. The coarser, less mature nature of the Glenrosa Section suggests source material is more proximal. This interpretation agrees with southerly paleocurrent measurements.

2. The Tranquille Formation lithofacies model associations from the McAbee beds include:

MB-MA1) The deposition of laterally discontinuous, irregularly-bounded, clast-supported conglomerates with lenses of imbricated pebbles occurred in a braided fluvial setting with proximal volcanics.

- MB-MA2) The deposition of organic-rich, microlaminated clays and thinly bedded, organic-rich to organic-poor siltstones and fine- to coarse-grained tuffaceous sandstones with normal grading, soft sedimentary deformation, and interbedded air-fall ash beds represents deposition of lacustrine strata, likely a result of episodic damming of a paleovalley with syndepositional volcanism or lacustrine fill cycles.
3. The Hardwick Sandstone Unit lithofacies model association from the basal conglomerate unit includes:
- PC-MA1) The deposition of laterally discontinuous, clast-supported, weakly to strongly imbricated conglomerates interbedded with normal graded sands, cross to planar stratified sands, and minor silt and ash fall beds occurred in multiple small channels with varied flow rates and depths in a shallow braided fluvial setting.
4. We recognize twelve chemically distinct ignimbrites that range in composition from andesite to rhyodacite. All but two samples show similar geochemical trends to previous bulk rock samples including the enrichment of the LREE relative to the HREE, the enrichment of the LILE concentrations, and the lack of a strong negative Eu anomaly. The two remaining samples show the most evolved magmatic signatures, including a large negative Eu anomaly that indicates plagioclase fractionation occurred prior to the eruption.
5. Based on the precise adakite definition of Castillo (2012), only five of the previously reported sixteen samples are considered adakites. The remaining eleven samples from the Kamloops, Penticton, and Princeton Groups are adakite-like and still suggest a primitive magmatic source. This study provides one additional sample from the Princeton Group that matches the new adakite REE criteria. True adakite signatures are only found in the Princeton Basin.
6. The new U/Pb zircon dates provide additional precision and accuracy to the timing of basin accumulation and the initiation of the ignimbrite flare-up. In the Republic Graben, the oldest ignimbrite date indicates that the ignimbrite flare-up initiated at 52.43 ± 0.55 Ma in the south, and at 51.00 ± 0.31 Ma in the Princeton and Kamloops Groups in the north. In addition, we argue the deposition of the famous fossil localities

in McAbee, Falkland, and Princeton provide a mid-latitude terrestrial fossil and climate record of high temperatures ($>12^{\circ}\text{C}$ higher than modern) and high $p\text{CO}_2$ during the EECO (52.6-50.3 Ma).

7. The measured $\delta\text{D}_{\text{glass}}$ values from southern British Columbia range from -82‰ to -197‰ . Our new depositional age constraints and stratigraphy indicate that this range of values is not solely due to a regional topographic changes or global climatic trends, but also to local hydrology variations including the enrichment of $\delta\text{D}_{\text{glass}}$ values due to deposition of ignimbrites into evaporative lacustrine systems.
8. Our $\delta\text{D}_{\text{glass}}$ data indicates a high standing ($2800\text{-}3000\text{ m} \pm 300\text{ m}$) hinterland plateau existed from at least $47.33 \pm 0.24\text{ Ma}$ to $50.20 \pm 1.00\text{ Ma}$. Our new model suggests previous stable isotope paleoaltimetry studies have overestimated Eocene elevations due to an underestimation of the regional isotopic lapse rate. In addition, paleoelevation estimates from paleofloral proxies, paleophysiography, and paleodrainage directions significantly underestimate paleoelevations by at least $\sim 1\text{ km}$.
9. Combined, these new data suggest a south to north trend in both the initiation of basin subsidence and ignimbrite flare-ups, and that a high-standing hinterland plateau existed concurrently with the ignimbrite flare-up event. Based on these results, we prefer the opening of a slab window as the mechanism driving magmatic and basin evolution within the southern Canadian Cordillera.

7.0 References

- Armstrong, R. L., 1988, Mesozoic and early Cenozoic magmatic evolution of the Canadian Cordillera, Geological Society of America Special Papers, v. 218, p. 55-92.
- Atwater, T., 1970, Implications of plate tectonics for the Cenozoic tectonic evolution of western North America, Geological Society of America Bulletin, v. 81, p.3513-3536.
- Babcock, R. S., Burmester, R. F., Engebretson, D. C., Warnock, A., and Clark, K. P., 1992, A rifted margin origin for the Crescent basalts and related rocks in the Northern Coast Range Volcanic Province, Washington and British Columbia, Journal of Geophysical Research, v. 97, p. 6799-821.
- Bao, X., Eaton, D. W., Guest, B., 2014, Plateau uplift in western Canada caused by lithospheric delamination along a craton edge, Nature Geoscience, v. 7, p. 830-833.
- Bardoux M., Mareschal, J. C., 1994, Extension in south-central British Columbia: mechanical and thermal controls, Tectonophysics, v. 238, p. 451-470.
- Beerling, D. J., and Royer, D. L., 2011, Convergent Cenozoic CO₂ history, Nature Geoscience, v. 4, p. 418-420.
- Best, M. G., Christiansen, E. H., de Siliva, S., Lipman, P. W., 2016, Slab-rollback ignimbrite flareups in the southern Great Basin and other Cenozoic American arcs: a distinct style of arc volcanism, Geosphere, v. 12, p. 1-39.
- Bourdon, E., Eissen, J. P., Gutscher, M. A., Monzier, M., Hall, M., and Cotton, J., 2003, Magmatic response to early aseismic ridge subduction: The Ecuadorian margin case (South America), Earth and Planetary Science Letters, v. 205, p. 123-138.
- Breitsprecher, K., Thorkelson, D., Groome, W., and Dostal, J., 2003, Geochemical confirmation of the Kula-Farallon slab window beneath the Pacific Northwest in Eocene time, Geology, v. 31, p. 351-354.
- Brown, S. R., 2010, Geology and Geochronology of the Southern Okanagan Valley Shear Zone, Southern Canadian Cordillera, British Columbia [Ph.D. thesis]: Burnaby, British Columbia, Canada, Simon Fraser University, 320 p.
- Brown, S. R., Gibson H. D., Andrews, G. D. M., Thorkelson, D. J., Marshall, D. D., Vervoort, J. D., and Rayner, N., 2012, New constraints on Eocene extension within the Canadian Cordillera and identification of Phanerozoic protoliths for footwall gneisses of the Okanagan Valley shear zone, Lithosphere, v. 4, p. 354-377.
- Brun, J-P., Faccenna, C., 2008, Exhumation of high-pressure rocks driven by slab rollback, Earth and Planetary Science Letters, v. 272, p. 1-7.

- Bunker B. C., 1994, Molecular mechanisms for corrosion of silica and silicate glasses, *Journal of Non-Crystal Solids*, v. 179, p. 300-308.
- Carroll, A., Bohacs, K. M., 1999, Stratigraphic classification of ancient lakes: Balancing tectonic and climatic controls, *Geology*, v. 27, p. 99-102.
- Cassel, E. J., Graham, S. A., Chamberlain, C. P., and Henry, C. D., 2012, Early Cenozoic topography, morphology, and tectonics of the northern Sierra Nevada and western Basin and Range, *Geosphere*, v. 8, p. 229–249.
- Cassel, E. J., Breecker, D. O., Christopher D. Henry, Toti E. Larson, and Daniel F. Stockli, 2014, Profile of a paleo-orogen: High Topography across the present-day Basin and Range from 40 to 23 Ma, *Geology*, v. 42, no. 11, p. 1007-1010.
- Cassel, E. J., and Breecker, D. O., 2017, Long-term stability of hydrogen isotope ratios in hydrated volcanic glass, *Geochimica et Cosmochimica Acta*, v. 200, p. 67-87.
- Cerling, T. E., Brown, F. H., and Bowman, J. R., 1985, Low-temperature alteration of volcanic glass: hydration, Na, K, ^{18}O and Ar mobility, *Chemical Geology: Isotope Geoscience Section*, v. 52, p.281-293.
- Chamberlain, C. P., Mix, H. T., Mulch, A., Hren, M. T., Kent-Corson, M. L., Davis, S. J., Horton, T. W., and Graham, S. A., 2012, The Cenozoic climatic and topographic evolution of the western North American Cordillera, *American Journal of Science*, v. 312, p. 213-262.
- Church, B. N., 1973, *Geology of the White Lake Basin: British Columbia Department of Mines and Petroleum Resources*, v. Bulletin 61, p. 3-141.
- Church, B. N., 1985, *Volcanology and structure of Tertiary outliers in southcentral British Columbia, Field Trip Guidebook*, B. C., Ministry of Energy, Mines, and Petroleum Resources, p. 5-46.
- Coney, P. J., and Harms, T. A., 1984, Cordilleran metamorphic core complexes: Cenozoic extensional relics of Mesozoic compression, *Geology*, v. 12, p. 550-554.
- Cubley, J. F., Pattison, D. R. M., Archibald, D. A., Jolivet, M., 2012, Thermochronological constraints on the Eocene exhumation of the Grand Forks complex, British Columbia, based on $^{40}\text{Ar}/^{39}\text{Ar}$ and apatite fission track geochronology, *Canadian Journal of Earth Science*, v. 50, p. 576-598.
- Dansgaard, W., 1964, Stable isotopes in precipitation: *Tellus A*, v.16.

- DeCelles, P. G., Carrapa, B., Horton, B., McNabb, J., Gehrels, G. E., and Boyd, J., 2015, The Miocene Arizaro Basin, central Andean hinterland, Response to partial lithosphere removal?, *Geological Society of America Memoirs*, v. 212, p. 359-386.
- Defant, M. J., and Drummond, M. S., 1990, Derivation of some modern arc magmas by melting of young subducted lithosphere. *Nature* v. 347, p. 662-885.
- Defant, M.J., and Kepezhinskas, P., 2001, Evidence suggests slab melting in arc magmas: *Eos (Transactions, American Geophysical Union)*, v. 82, p. 65-69.
- Dostal, J., Breitsprecher k., Church, B. N., Thorkelson, D., and Hamilton, T. S., 2003, Eocene melting of Precambrian lithospheric mantle: Analcime-bearing volcanic rocks from the Challis-Kamloops belt of south central British Columbia, *Journal of Volcanology and Geothermal Research*, v. 126, p. 303-326.
- Ducea, M. N., Seclaman, A., Murray, K., Jianu, D., and Schoenbohm, L., 2013, Mantle-drip magmatism beneath the Altiplano-Puna Plateau, central Andes, *Geology*, v. 41, p. 915-918.
- Evans, J. E., 1991, Paleoclimatology and paleobotany of the Eocene Chumstick formation, Cascade Range, Washington (USA): A rapidly subsiding alluvial basin, *Paleogeography, Paleoclimatology, Paleoecology*, v. 88, p. 239-264.
- Ewing, T. E., 1981, Petrology and geochemistry of the Kamloops Group volcanics, British Columbia, *Canadian Journal of Earth Sciences*, v. 18, p. 1478-1491.
- Feng, R., Poulsen, C. J., Werner, M., Chamberlain, C. P., Mix, H. T., Mulch, A., 2013, Early Cenozoic evolution of topography, climate, and stable isotopes in precipitation in the North American Cordillera, *American Journal of Science*, v. 313, p. 613-648.
- Friedman, R., Mahoney, J., and Cui, Y., 1995, Magmatic evolution of the southern Coast Belt: Constraints from Nd-Sr isotopic systematics and geochronology of the southern Coast Plutonic Complex, *Canadian Journal of Earth Sciences*, v. 32, p. 1681-1698.
- Friedman, I., Gleason, J., Sheppard, R. A., and Gude, A. L., 1993, Deuterium fractionation as water diffuses into silicic volcanic ash, *Climate change in continental isotopic records*, p. 321-323.
- Galewsky, J., 2009, Orographic precipitation isotopic ratios in stratified atmospheric flows: Implications for paleoelevation studies: *Geology*, v. 37, p. 791-794.
- Gao, S., et al., 2004, Recycling lower continental crust in the North China craton, *Nature*, v. 432, p. 933-938.

- Ghosh, D. K., 1995, Nd-Sr isotopic constraints on the interactions of the Intermontane Superterrane with the western edge of North America in the southern Canadian Cordillera, *Canadian Journal of Earth Sciences*, v. 32, p. 1740-1758.
- Göğüş, O. H., and Pysklywec, R. N., 2008, Near-surface diagnostics of dripping or delaminating lithosphere: *Journal of Geophysical Research*, v. 113, p. 311-404.
- Goodwin, J. T., Surdam, R. C., 1967, Zeolitization of tuffaceous rocks of the Green River Formation, Wyoming, *Science*, v. 157, p. 307-308.
- Greenwood, D. R., Archibald, S. B., Mathewes, R. W., and Moss, P. T., 2005, Fossil biotas from the Okanagan Highlands, southern British Columbia and northeastern Washington State: climates and ecosystems across an Eocene landscape, *Canadian Journal of Earth Sciences*, v. 42, p. 167-185.
- Greenwood, D. R., and Wing, S. L., 1995, Eocene continental climates and latitudinal temperature gradients, *Geology*, v. 23, p. 1044-1048.
- Gordon, S. M., Whitney, D. L., Teyssier, C., Grove, M., Dunlap, W. J., 2008, Timescales of migmatization, melt crystallization, and cooling in a Cordilleran gneiss dome: Valhalla complex, southeastern British Columbia, *Tectonics*, v. 27, p. 1-28.
- Hardebol, N. J., Pysklywec, R. N., Stephenson, R., 2012, Small-scale convection at a continental back-arc to craton transition: Application to the southern Canadian Cordillera, *Journal of Geophysical Research*, v. 117, B01408.
- Haeussler, P. J., Bradley, D., Goldfarb, R., and Snee, L., 1995, Link between ridge subduction and gold mineralization in southern Alaska, *Geology*, v. 23, p. 995-998.
- Haeussler, P. J., Bradley, D. C., Wells, R. E., and Miller, M. L., 2003, Life and death of the Resurrection plate: Evidence for its existence and subduction in the northeastern Pacific in Paleocene-Eocene time, *Geological Society of America Bulletin*, v. 115, p. 867-880.
- Hills, L. V., and Baadsgaard, H., 1967, Potassium-argon dating of some lower Tertiary strata in British Columbia, *Bulletin Canadian Petroleum Geology*, v. 15, no. 2, p. 138-149.
- Hollister, L. S., 1982, Metamorphic evidence for rapid (2mm/yr) uplift of a part of the Central Gneiss Complex, Coast Mountains, B.C., *Canadian Mineralogist*, v. 20, p. 319-332.
- Huber, M., and R. Caballero (2003), Eocene El Nino: Evidence for robust tropical dynamics in the "hot-house," *Science*, v. 299, p. 877-881.

- Humphreys, E., 2009, Relation of flat subduction to magmatism and deformation in the western United States, *Geological Society of America Memoirs*, v. 204, p. 85-98.
- IAEA/WMO, 2015, Global Network of Isotopes in Precipitation. The GNIP Database.
- Ickert, R. B., Thorkelson, D. J., Marshall, D. D., and Ullrich, T. D., 2007, Eocene adakitic volcanism in southern British Columbia: remelting of arc basalt above a slab window, *Tectonophysics*, v. 464, p. 164-185.
- Kay, R. W., 1978, Aleutian magnesian andesites: melts from subducted Pacific Ocean crust, *Journal of Volcanology and Geothermal Research*, v. 4, p. 497-522.
- Laberge, J. D., and Pattison, D. R. M., 2007, Geology of the western margin of the Grand Forks complex, southern British Columbia: high-grade Cretaceous metamorphism followed by early Tertiary extension on the Granby fault, *Canadian Journal of Earth Science*, v. 44, p. 199-228.
- Lemieux, Y., Thompson, R., Erdmer, P., Simonetti, A., and Creaser, R., 2007, Detrital zircon geochronology and provenance of Late Proterozoic and mid-Paleozoic successions outboard of the miogeocline, southeastern Canadian Cordillera, *Canadian Journal of Earth Sciences*, v. 44, p. 1675-1693.
- Lowe, D. J., 2011, Tephrochronology and its application: A review, *Quaternary Geochronology*, v. 6., p. 107-153.
- Ludwig, K. R., 2012, User's Manual for Isoplot/Ex Version 4.1, A Geochronological Toolkit for Microsoft Excel, Berkeley Geochronology Center Spec, Pub. 5.
- Macpherson, C. G., Hall, R., 2002, Timing and tectonic controls in the evolving orogen of SE Asia and the western Pacific and some implications for ore generation, In: Blundell, D. J., Neubauer, F., von Quadt, A. (eds), *The Timing and Location of Major Ore Deposits in an Evolving Orogen*, Geological Society, London, p. 49-67.
- Madsen, J. K., Thorkelson, D. J., Friedman, R. M., Marshall, D. D., 2006, Cenozoic to Recent plate configurations in the Pacific Basin: ridge subduction and slab window magmatism in western North America, *Geosphere* 2, v. 1, 11-34.
- Maill, A. D., 1996, *The geology of fluvial deposits: Sedimentary facies, basin analysis, and petroleum geology*, Springer, p.1-524.
- McClaghry, J. D., and Gaylord, D. R., 2005, Middle Eocene sedimentary and volcanic infilling of an evolving supradetachment basin: White Lake Basin, southcentral British Columbia, *Canadian Journal of Earth Sciences*, v. 42, p. 49-66.

- Mercier, J. -P., Bostock, M. G., Cassidy, J. F., Dueker, K., Gaherty, J. B., Garnero, E. J., Revenaugh, J., Zandt, G., 2009, Body-wave tomography of western Canada, *Tectonophysics*, v. 475, p. 480-492.
- Mix, H. T., Mulch, A., Kent-Corson, M. L., Chamberlain, C.P., 2010, Cenozoic migration of topography in the North American Cordillera, *Geology*, v. 39, p. 87-90.
- Monger, J. W. H., 1968, Early Tertiary stratified rocks, Greenwood map-area, (82 E/2) British Columbia: Canada Geological Survey Paper, v. 67-42, p. 1-39.
- Monger, J. W. H., Price, R. A., and Tempelman-Kluit, D. J., 1982, Tectonic accretion and the origin of the two major metamorphic and plutonic belts in the Canadian Cordillera, *Geology*, v. 10, p. 70-75.
- Monger, J. W. H., 1985, Structural evolution of the southwestern Intermontane belt, Ashcroft and Hope map areas, British Columbia, Current Research, Geological Survey of Canada, v. 85-1A, p.349-358.
- Morris, G. A., Larson, P. B., and Hooper, P. R., 2000, "Subduction style" magmatism in a nonsubduction setting: The Colville Igneous Complex, northeast Washington State, USA, *Journal of Petrology*, v. 41, p. 43-67.
- Moye, F. J., Hackett, W. R., Blakley, J. D., and Snider, L. G., 1988, Regional geologic setting and volcanic stratigraphy of the Challis volcanic field, central Idaho, in Link, P.K., and Hackett, W.R., editors, *Guidebook to the Geology of Central and Southern Idaho*, Idaho Geological Survey Bulletin 27, pp. 87-97.
- Mulch, A., Teyssier, C., Cosca, M., and Chamberlain, C., 2007, Stable isotope paleoaltimetry of Eocene core complexes in the North American Cordillera, *Tectonics*, v. 26.
- Mulch, A., Sarna-Wojcicki, A., Perkins, M., and Chamberlain, C., 2008, A Miocene to Pleistocene climate and elevation record of the Sierra Nevada (California), *Proceedings of the National Academy of Sciences*, v. 105, p. 6819-6824.
- Mustoe, G. E., and Gunnaway, W. L., 1997, Paleogeography and paleontology of the early Tertiary Chuckanut Formation, northwest Washington. *Washington Geology*, v. 25, p. 3-18.
- Mustoe, G. E., 2005, Diatomaceous origin of siliceous shale in Eocene lake beds of central British Columbia, *Canadian Journal of Earth Sciences*, v. 42, p. 231-241.
- Parrish, R. R., Carr, S. D., and Parkinson, D. L., 1988, Eocene extensional tectonics and geochronology of the southern Omineca Belt, British Columbia and Washington, *Tectonics*, v. 7, p. 181-212.

- Pearson, R. C., 1967, Geological map of the Bodie Mountain quadrangle, Ferry and Okanogan Counties, Washington: U.S. Geological Survey Geology Quadrangle Map GQ-636.
- Pearson, R. C., and Obradovich, J. D., 1977, Eocene Rocks in Northeast Washington – Radiometric Ages and Correlation, Geological Survey Bulletin, v. 1433, p. 1-48.
- Peppe, D. J., Royer, D. L., Wilf, P., and Kowalski, E. A., 2010, Quantification of large uncertainties in fossil leaf paleoaltimetry, *Tectonics*, v. 29.
- Poage, M.A., and Chamberlain, C. P., 2001, Empirical relationships between elevation and the stable isotope composition of precipitation and surface waters: Considerations for studies of paleoelevation change: *American Journal of Science*, v. 301, p. 1-15.
- Poulsen, C. J., and Jeffery, M. L., 2011, Climate change imprinting on stable isotopic compositions of high-elevation meteoric water cloaks past surface elevations of major orogens: *Geology*, v. 39, p. 595-598.
- Price, R. A., and Mountjoy, E. W., 1970, Geologic structure of the Canadian Rocky Mountains between Bow and Athabasca Rivers-A progress report: Geological Association of Canada Special Paper 6, p. 7-25.
- Price, R. A., 1981, The Cordilleran Foreland Thrust and Fold Belt in the Southern Canadian Rocky Mountains, in McClay, K.R., and Price, N. J., eds., *Thrust and Nappe Tectonics*, The Geological Society, p. 427-448.
- Price, R. A., 1986, The southeastern Canadian Cordillera: thrust faulting, tectonic wedging, and delamination of the lithosphere, *Journal of Structural Geology*, v. 8, p. 239-254.
- Read, P. B., 2000, *Geology of Princeton and Tulameen Basins*, GeoFile 2000-3: Vancouver, British Columbia, Ministry of Energy and Mines, p. 12.
- Russo, R. M., VanDecar, J. C., Comte, D., Mocanu, V. I., Gallego, A., Murdie, R. E., 2010, Subduction of the Chile Ridge: Upper mantle structure and flow, *GSA Today*, v. 20., p. 4-10.
- Simony, P. S., and Carr, S.D., 2011, Cretaceous to Eocene evolution of the southeastern Canadian Cordillera: Continuity of Rocky Mountain thrust systems with zones of “in-sequence” mid-crustal flow, v. 33, p.1417-1434.
- Sisson, V. R., Pavlis, T. L., Roeske, S. M., Thorkelson, D. J., 2003, Introduction: An overview of ridge-trench interactions in modern and ancient settings, *GSA Special Paper*, v. 371, p. 1-18.

- Salaun, A., Villemant, B., Gerard, M., Komorowski, J. C., Michel, A., 2011, Hydrothermal alteration in andesitic volcanoes: Trace element redistribution in active and ancient hydrothermal systems of Guadeloupe (Lesser Antilles), *Journal of Geochemical Exploration*, v. 111, p. 59-83.
- Slama, J., Kosler, J., Condon, D. J., Crowley, J. L., Gerdes, A., Hanchar, J. M., Horstwood, M. S. A., Morris, G. A., Nasdala, L., Norberg, N., Schaltegger U., Schoene, B., Tubrett, M. N., Whitehouse, M. J., 2008, Plesovice zircon – A new natural reference material for U – Pb and Hf isotopic microanalysis, *Chemical Geology*, v. 249, p. 1-35.
- Rittenhouse-Mitchell, K. J., 1997, Sedimentology, stratigraphy, and tectonic setting of the Eocene Springbrook Formation, southcentral British Columbia. M.Sc. thesis, Washington State University, Pullman, Washington.
- Rouse, G. E., and Mathews, W. H., 1961, Radioactive dating of Tertiary plant-bearing deposits, *Science*, v. 133, no. 3458, p. 1079-1080.
- Rowley, D. B., 2007, Stable isotope-based paleoaltimetry: Theory and validation, *Reviews in Mineralogy and Geochemistry*, v. 66, p. 23–52.
- Sarna-Wojcicki, A., and Davis, J., 1991, Quaternary Tephrochronology, *Quaternary Nonglacial Geology: Conterminous US*, The Geology of North America, Geological Society of America, Boulder, p. 3-116.
- Smith, M.E., Carroll, A. R., Singer, B. S., 2008, Synoptic reconstruction of a major ancient lake system: Eocene Green River Formation, western United States, *GSA Bulletin*, v. 120, p. 54-84.
- Smith, R. Y., Basinger, J. F., Greenwood, D. R., 2009, Depositional setting, fossil flora, and paleoenvironment of the Early Eocene Falkland site, Okanagan Highlands, British Columbia, *Canadian Journal of Earth Science*, v. 46, p. 811-822.
- Smith, R. Y., Greenwood, D. R., and Basinger J. F., 2010, Estimating paleoatmospheric $p\text{CO}_2$ during the Early Eocene Climatic Optimum from stomatal frequency of Ginkgo, Okanagan Highlands, British Columbia, Canada, *Journal of Paleogeography, Paleoclimatology, Paleoecology*, v. 293, p. 120-131.
- Smith, M. E., Carroll, A. R., Jicha, B. R., Cassel, E. J., and Scott, J. J., 2014, Paleogeographic record of Eocene Farallon slab rollback beneath western North America, *Geology*, v. 42, p. 1039-1042.

- Sun, S. S., and McDonough, W. F., 1989, Chemical and isotopic systematics of oceanic basalts: implication for mantle composition and processes, Geological Society Special Publications, v. 42, p. 313-345.
- Thorkelson, D. J., 1989, Eocene sedimentation and volcanism in the Fig Lake Graben, southwestern British Columbia, Canadian Journal of Earth Sciences, v. 26, p. 1368-1373.
- Thorkelson D. J., and Taylor, R. P., 1989, Cordilleran slab windows, Geology, v. 17, p. 47-63.
- Thorkelson, D. J., 1996, Subduction of diverging plates and the principles of slab window formation, Tectonophysics, v. 255, p. 47-63.
- Thorkelson, D. J., Breitsprecher, K., 2005, Partial melting of slab window margins: genesis of adakitic and non-adakitic magmas, Lithos, v. 79, p. 25-41.
- Tribe, S., 2005, Eocene paleo-physiography and drainage directions, southern Interior Plateau, British Columbia, Canadian Journal of Earth Sciences, v. 42, p. 215-250.
- Vanderhaeghe, O., Teyssier, C., McDougall, I., and Dunlap, W. J., 2003, Cooling and exhumation of the Shuswap Metamorphic Core Complex constrained by $^{40}\text{Ar}/^{39}\text{Ar}$ thermochronology, GSA Bulletin, v. 115, p. 200-216.
- Villeneuve, M. E., and Mathewes, R., 2005, An early Eocene age for the Quilchena fossil locality, southern British Columbia, Current Research, Geological Survey of Canada, 2005-A4, p. 1-9
- Wernicke, B., Clayton R., Ducea, M., Jones, C. H., Park S., Ruppert S., Saleeby, J., Snow, J. K., Squires, L., Fliedner, M., Jiracek, G., Keller, R., Klemperer, S., Luetgert, J., Malin, P., Miller, K., Mooney, W., Oliver, H., Phinney, R., 1996, Origin of high mountains in the continents: The southern Sierra Nevada, Science, v. 271, p. 190-193.
- Wolfe, J. A., and Wehr, W. C., 1987, Middle Eocene dicotyledonous plants from Republic, northeastern Washington, United States Geological Survey Bulletin, v. 1587, p. 1-25.
- Wolfe, J. A., 1994, Tertiary climatic changes at middle latitudes of western North America, Paleogeography, Paleoclimatology, Paleoecology, v. 108, p. 195-205.
- Wolfe, J. A., Forest, C. E., and Molnar, P., 1998, Paleobotanical evidence of Eocene and Oligocene paleoaltitudes in midlatitude western North American, Geological Society of America Bulletin, v. 110(5). P. 664-678.
- Yonge, C. J., Goldenberg, L., and Krouse, H. R., 1989, An isotope study of water bodies along a traverse of southwestern Canada, Journal of Hydrology, v. 106, p. 245-255.

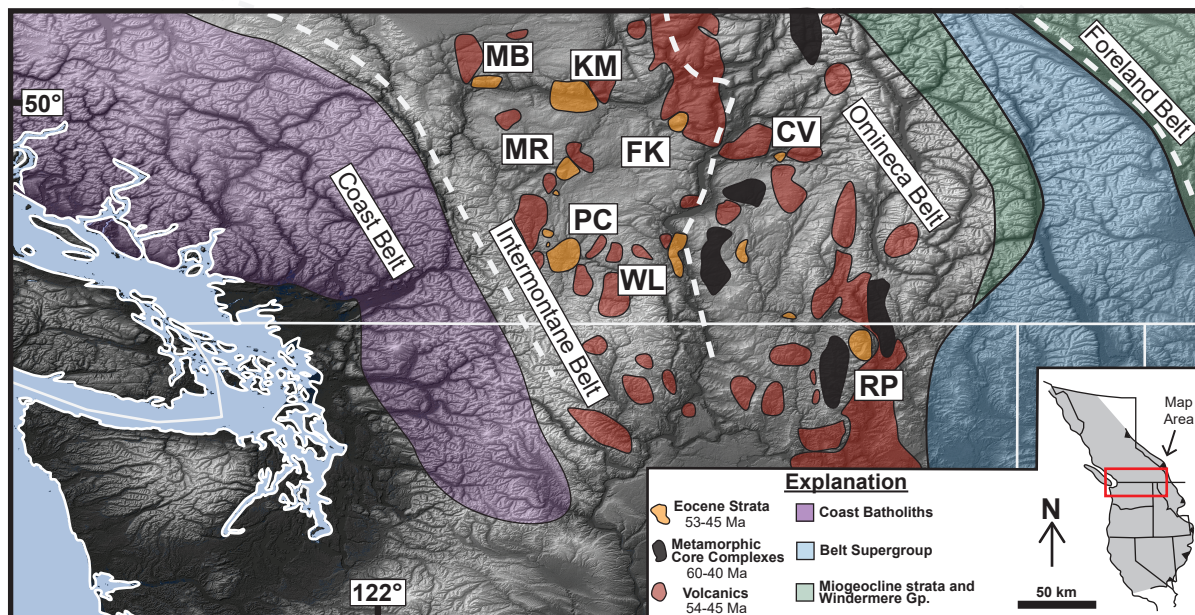


Figure 2.1. Overview map highlighting the key features of the study area in northern Washington (WA) and southern British Columbia (BC). Dashed lines indicate morphogeological belt boundaries. Age constraints of the Coast Belt from Friedman et al. (1995). Age constraints of the volcanics from Rouse and Mathews (1961), Hills and Baadsgaard (1967), Pearson and Obradovich (1977), Read (2000), Villeneuve and Mathewes (2005), and Ickert et al. (2007). Eocene fluvial and lacustrine strata are in Republic (RP), White Lake (WL), Kelowna (KL), Falkland (FK), Creighton Valley (CV), McAbee (MB), Merritt (MR), and Princeton (PC). Age constraints of the metamorphic core complexes from Vanderhaeghe et al. (2002), Laberge and Pattison (2007), Gordon et al. (2008), and Cubley et al. (2013).

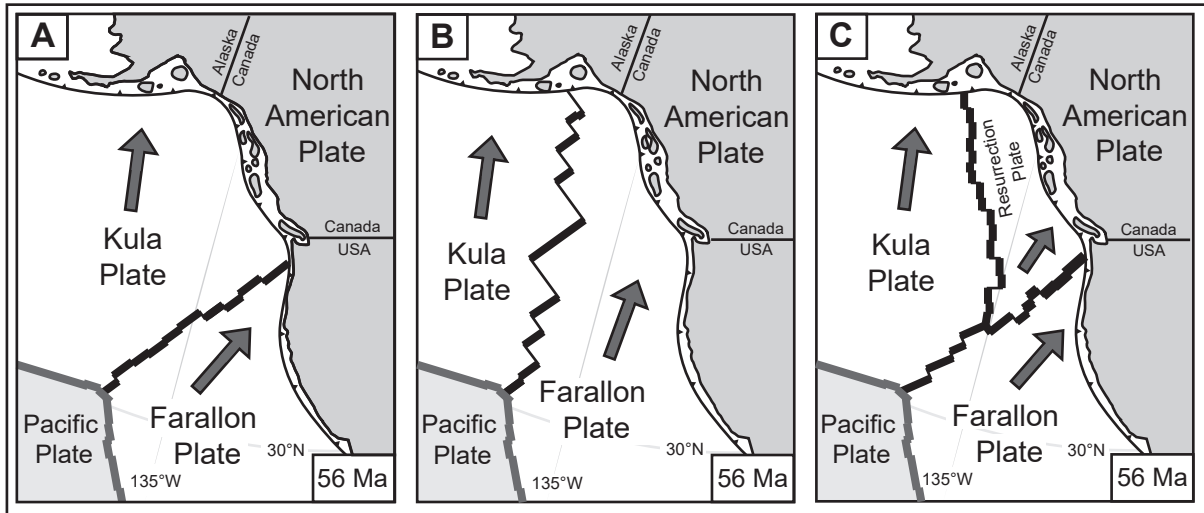


Figure 2.2. Proposed plate reconstructions at ~56 Ma to explain Eocene magmatism, core complex exhumation, and basin formation. Orientation of spreading ridges are speculative. Figures 2A and 2B show Kula-Farallon triple junction in northern Washington and Alaska, respectively (e.g. Thorkelson and Taylor, 1989; Haeussler et al., 1995). Figure 3A shows two triple junctions uniting the two previous hypotheses (Haeussler et al., 2003). Modified from Haeussler et al. (2003).

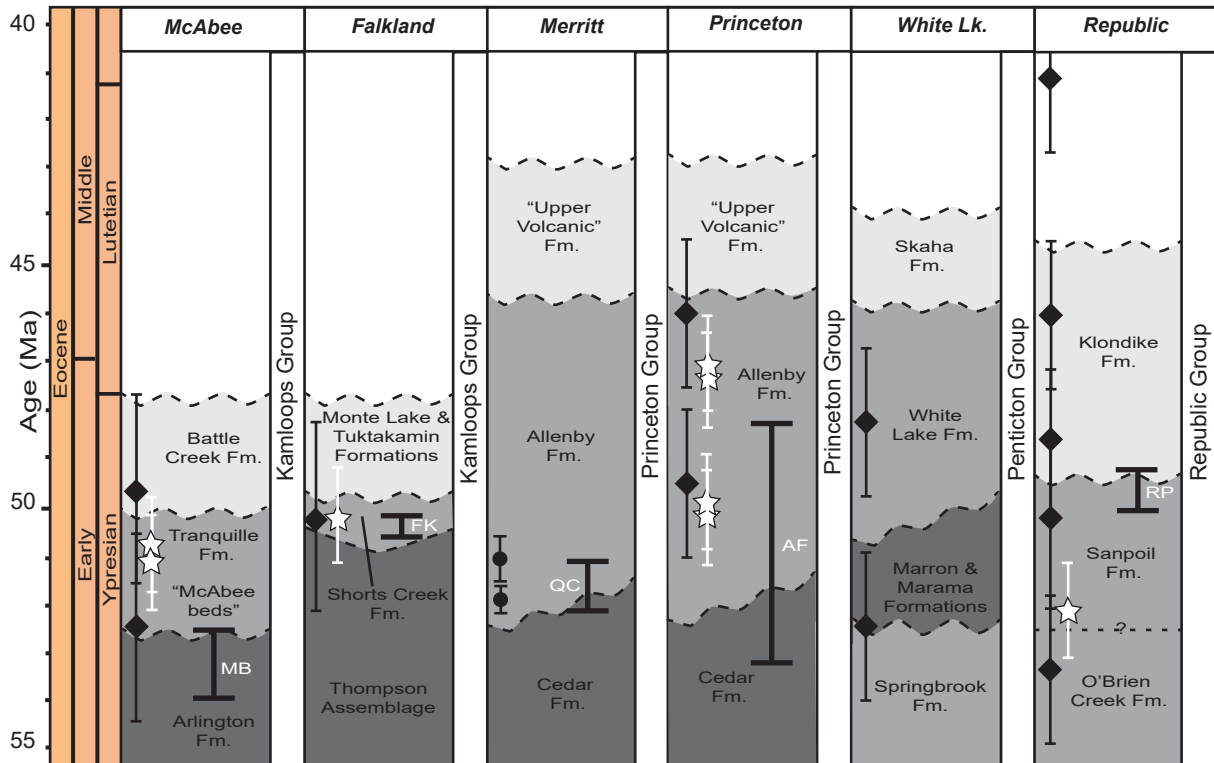
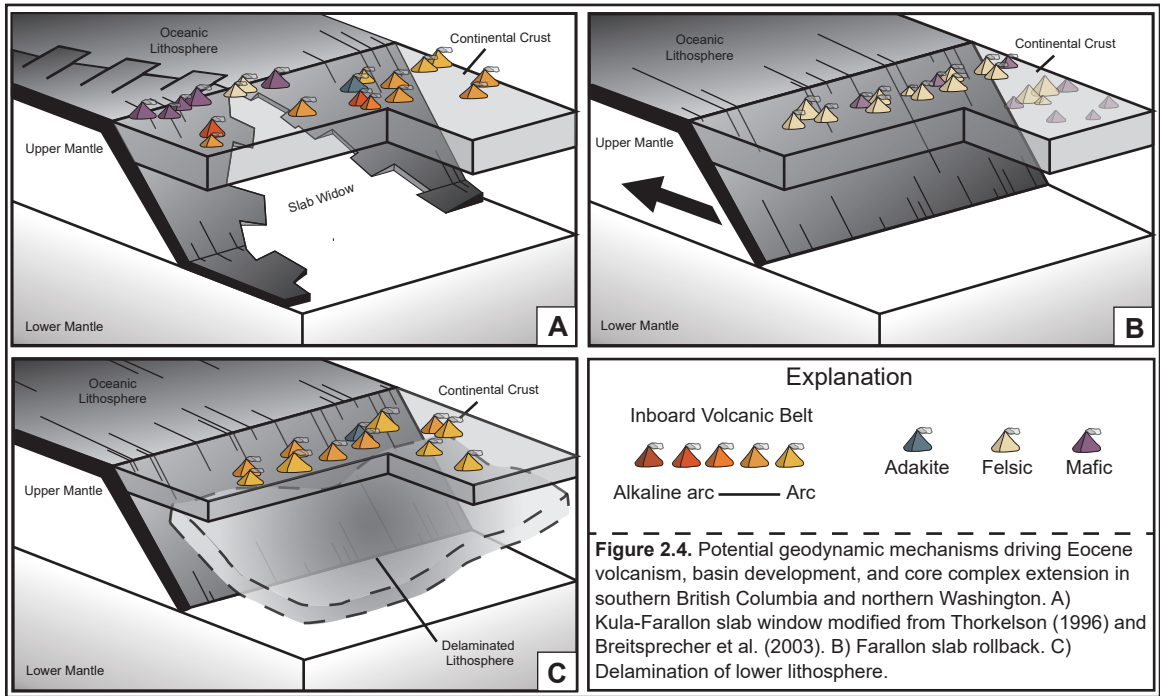


Figure 2.3. Overview of the regional stratigraphic and nomenclature correlation of the study area from Church (1973), McClaughry and Gaylord (2005), Mustoe (2005), Greenwood et al. (2005), Read (2000), Ewing (1981), and Pearson and Obradovich (1977). Dashed lines indicate uncertain age constraints. Curved dashed lines represent unconformities. Dark gray represents older basalts, andesites, and rhyolites. Medium gray indicates interbedded fluvial, lacustrine, and rhyolite to andesite ignimbrite strata. Light gray indicates younger volcanic breccias and rhyolite to andesite flows. The diamonds represent previous K/Ar dating. The circles indicate previous $^{40}\text{Ar}/^{39}\text{Ar}$ dating. The stars represent U/Pb zircon dating from this study. The bold black brackets from Greenwood et al. (2016) indicate previous age correlations of the McAbee beds (MB), FK (Falkland), Quilchena (QC), Allenby Formation (AF), and Republic (RP). Ages of the Allenby Formation from sources cited in Read (2000) and Princeton Group volcanics from Ickert et al. (2007). Age of Quilchena from $^{40}\text{Ar}/^{39}\text{Ar}$ and U/Pb dating from Villeneuve and Mathewes (2005). Dates for Falkland, Republic, and the Princeton Chert beds within the Allenby Formation from Archibald et al. (2010), Moss et al. (2005), and DeVore and Pigg (2010). But these citations do not provide the original radiometric dating results. Further investigation reveals these citations are referencing unpublished data from abstracts or personal communications.



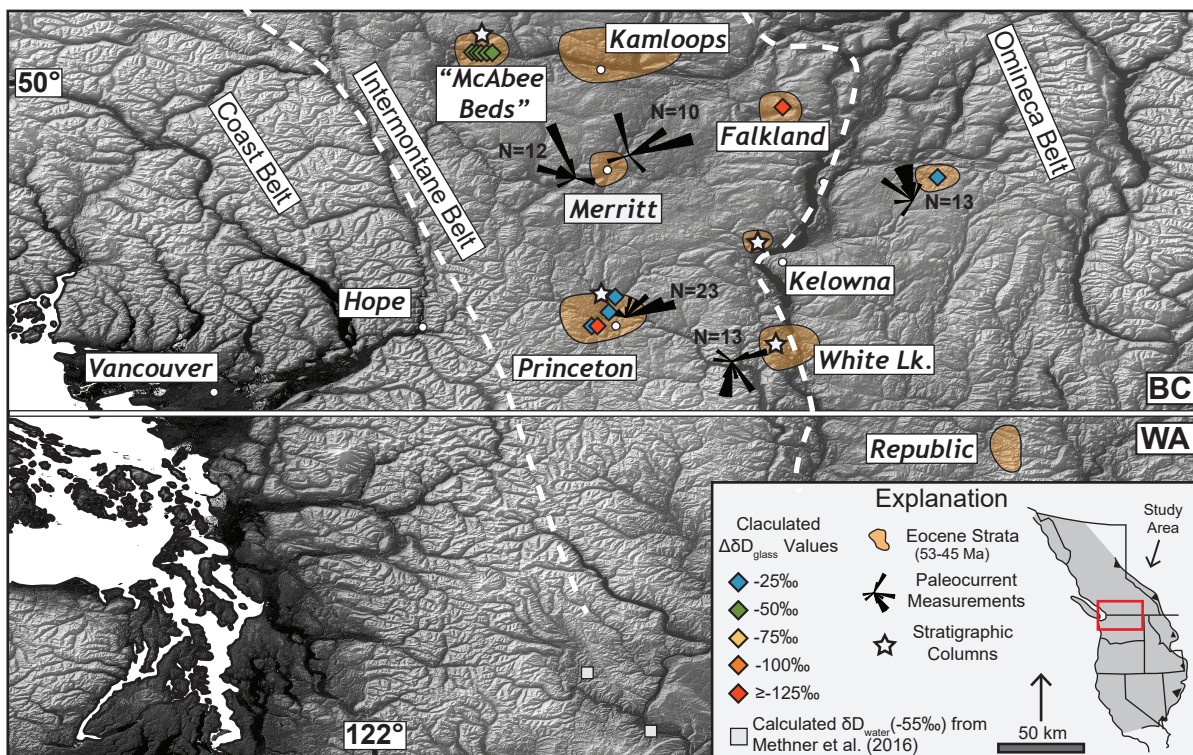


Figure 4.1. Overview map highlighting key δD_{glass} and paleocurrent results. Dashed lines represent the morphogeological belt boundaries. Dates of the volcanics from Rouse and Mathews (1961), Hills and Baadsgaard (1967), Pearson and Obradovich (1977), Read (2000), Villeneuve and Mathewes (2005), Ickert et al. (2007). δD_{glass} values converted to $\Delta\delta D_{\text{glass}}$ by normalizing δD_{glass} values to calculated δD_{water} value of -64‰ from Methner et al. (2016).

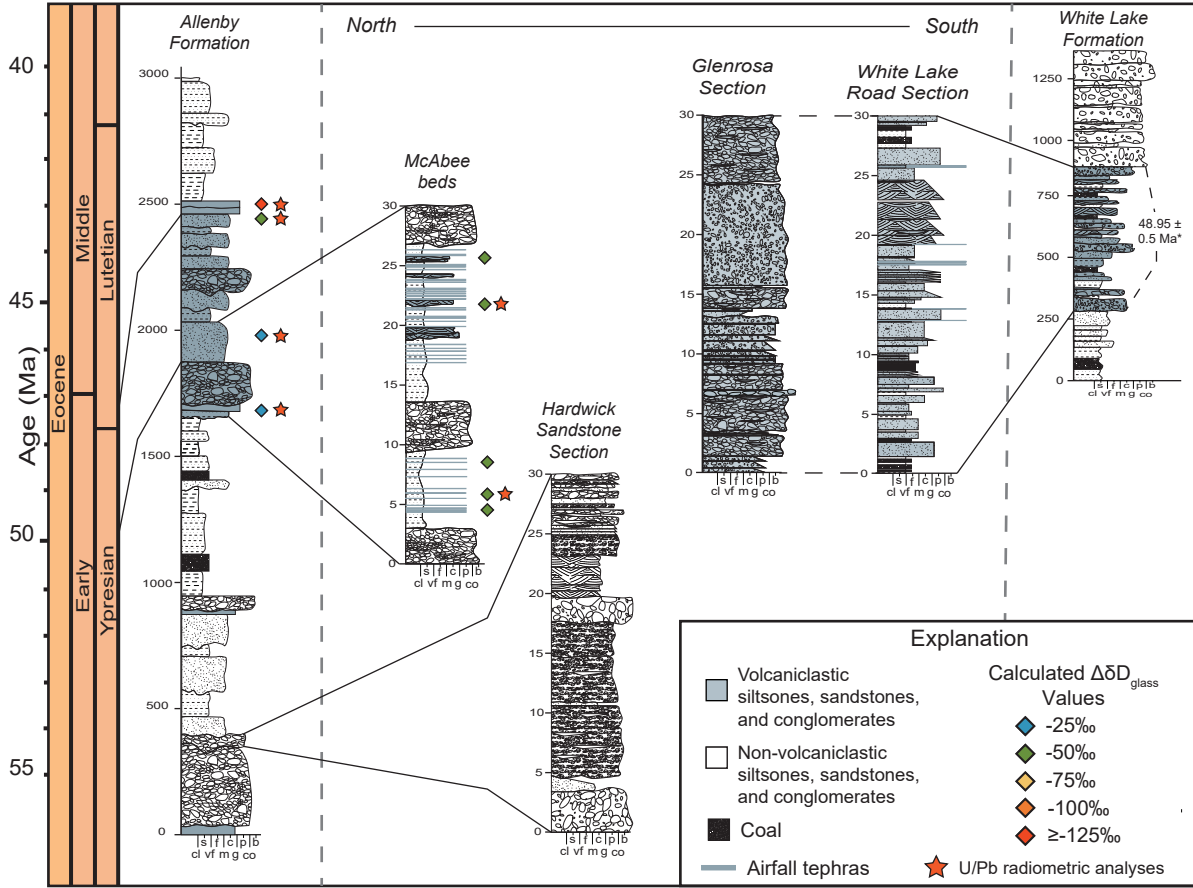


Figure 4.2. Correlated generalized and representative stratigraphic columns from the Kampoops, Pentiction, and Princeton Groups. Generalized White Lake Formation stratigraphy from McClaughry and Gaylord (2005). Generalized Allenby Formation stratigraphy from Read (2000). δD_{glass} values converted to $\Delta\delta D_{\text{glass}}$ by normalizing δD_{glass} values to calculated δD_{water} value of -64‰ from Methner et al. (2016). White Lake Formation date* based on preliminary U/Pb zircon analyses by Leier et al. (in prep).

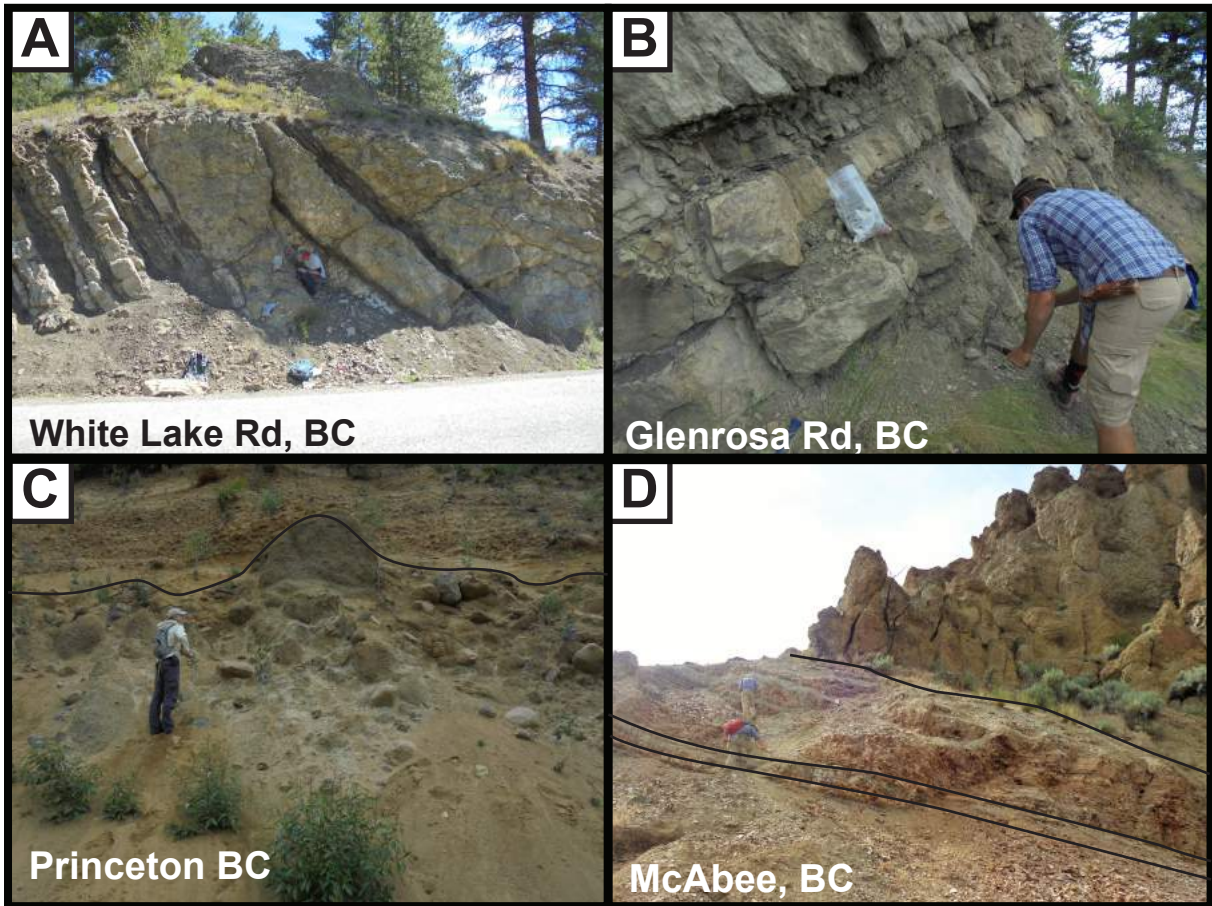


Figure 4.3. Characteristic photos from each measured stratigraphic section. (A) Interbedded silts and conglomerates of White Lake Fm. on White Lake Rd. (B) Interbedded silts and sands of the White Lake Fm. at Glenrosa. (C) Conglomerates and sands of the basal member of the Hardwick Sandstone Unit in the Allenby Fm. north of Princeton, BC. (D) Interbedded silts and sands with overlying conglomerates of the McAbee beds in the Kamloops Group.

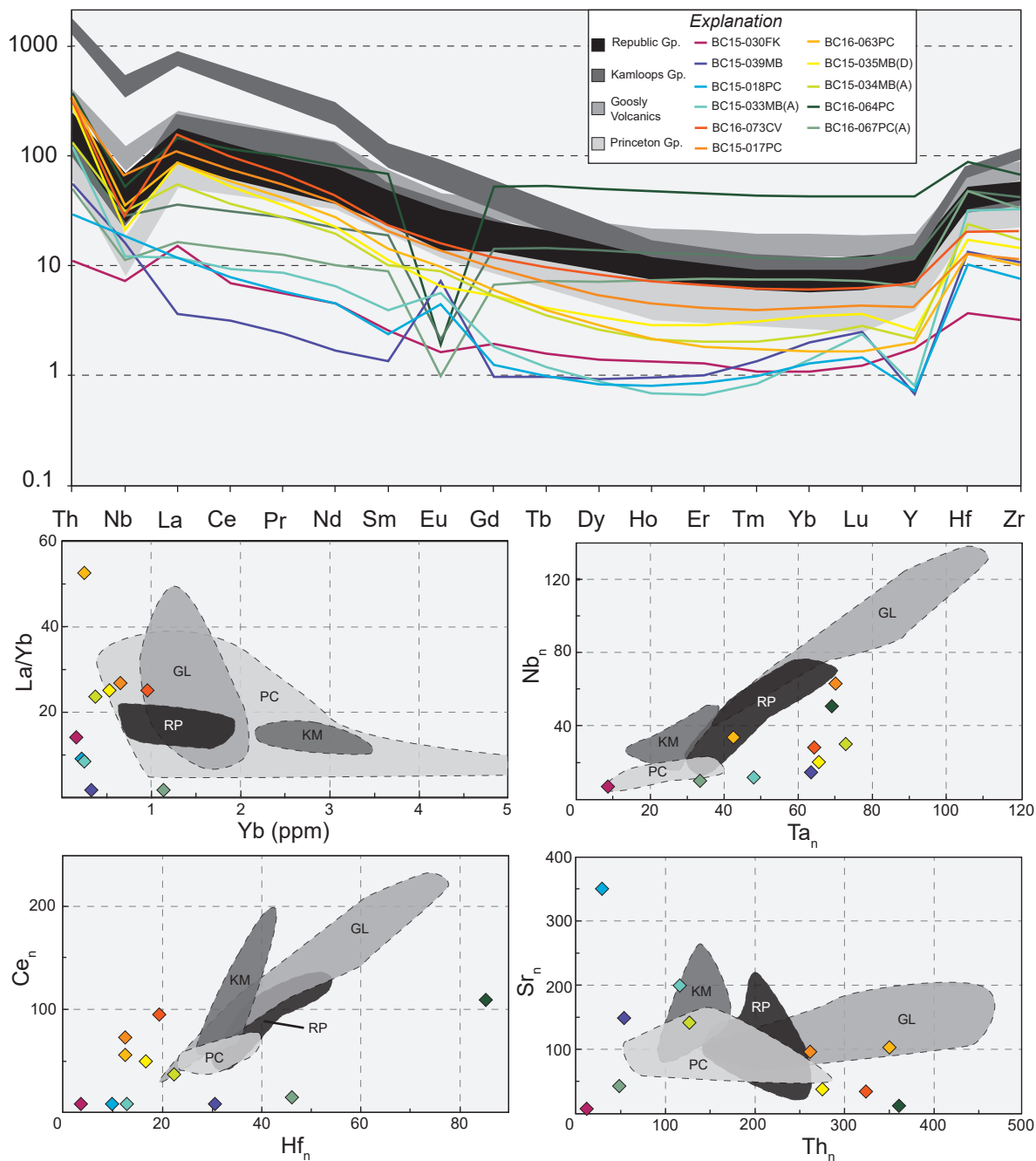


Figure 4.4. Comparison of trace and REE compositions of volcanic glasses and regional bulk rock compositions of volcanics from Morris et al. (1999), Ickert et al. (2007), Breitsprecher (2003), and Dostal (2001). Grey to black box indicate bulk rock REE data from Princeton (PC), Republic (RP), Kamloops (KM), and Goosly Volcanics (GL). Colored diamonds indicate volcanic glass samples from this study. (A) Chondrite-normalized trace and REE patterns show regional bulk rock geochemical trends (grey), Group #1 (yellow), Group #2 (blue), and Group #3 (green). (B-E) individual chondrite-normalized element concentrations and ratios.

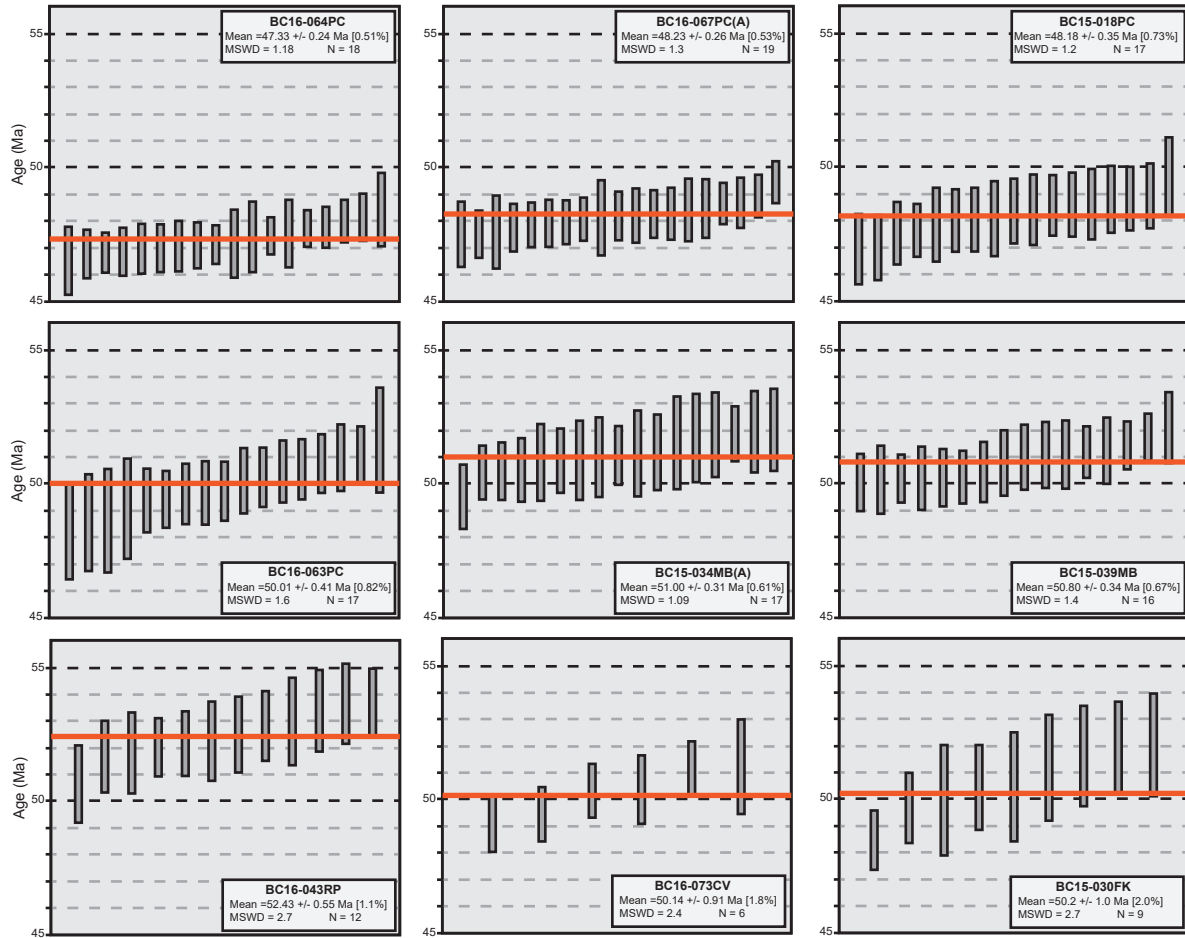


Figure 4.5. Comparison of the new weighted mean ages (max depositional ages) of ignimbrite samples BC15-018PC, BC16-063PC, BC16-064PC, BC16-067PC(A), BC15-034MB(A), BC15-039MB(D), BC16-043RP, BC16-073CV, and BC15-030FK. The orange line indicates calculated weighted mean age of each sample. Height of the grey boxes indicate the error on each zircon analysis.

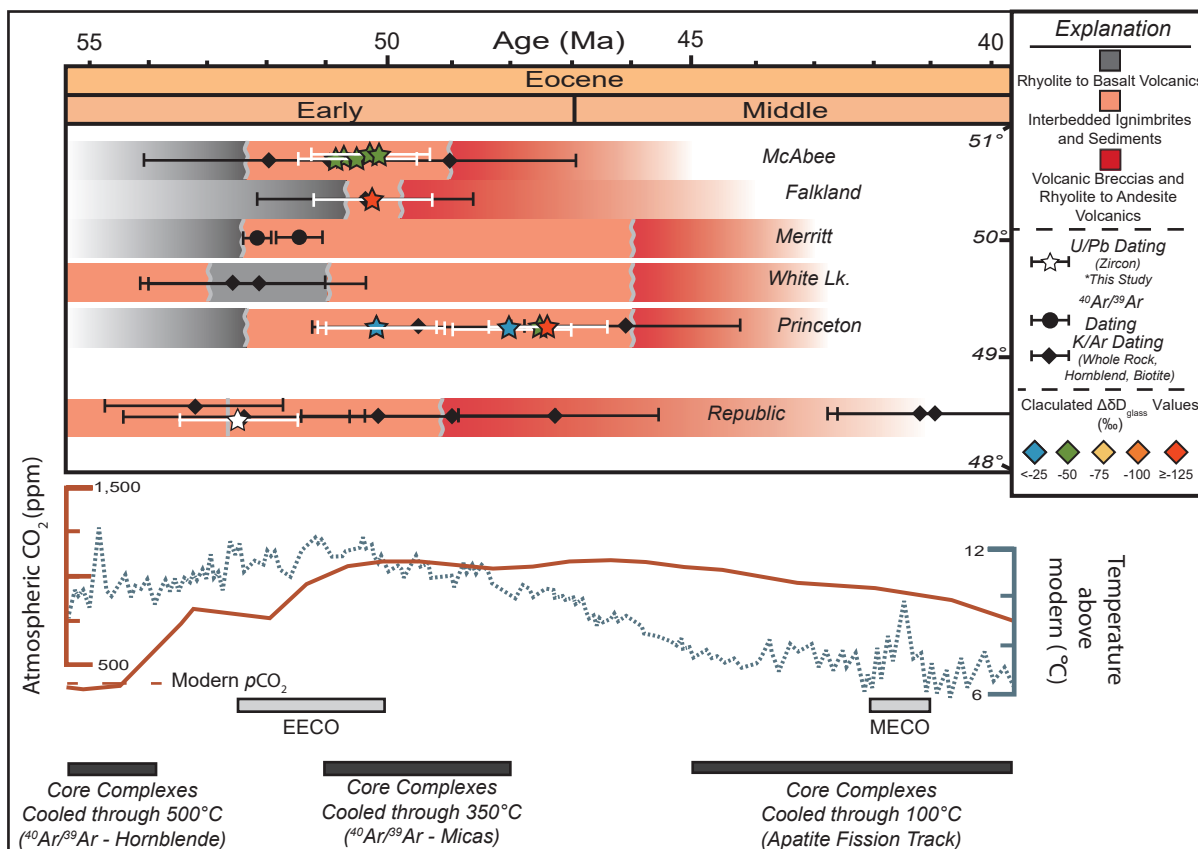


Figure 4.6. Overview of the regional stratigraphic correlation with previous age assignments, new U/Pb zircon radiometric dating results, and volcanic glass stable isotope results. $\delta\text{D}_{\text{glass}}$ values converted to $\Delta\delta\text{D}$ by normalizing $\delta\text{D}_{\text{glass}}$ values to calculated $\delta\text{D}_{\text{water}}$ value of -55‰ from Methner et al. (2016). Age constraints of the volcanics from Rouse and Mathews (1961); Hills and Baadsgaard (1967), Pearson and Obradovich (1977), Read (2000), Villeneuve and Mathews (2005), and Ickert et al. (2007). Eocene $p\text{CO}_2$ and temperature curves from Beerling and Royer (2011) and Zachos et al. (2008), respectively. Regional core complex ages from Vanderhaeghe et al. (2002), Gordon et al. (2008), Cubley et al. (2013), and Laberge and Pattison (2007).

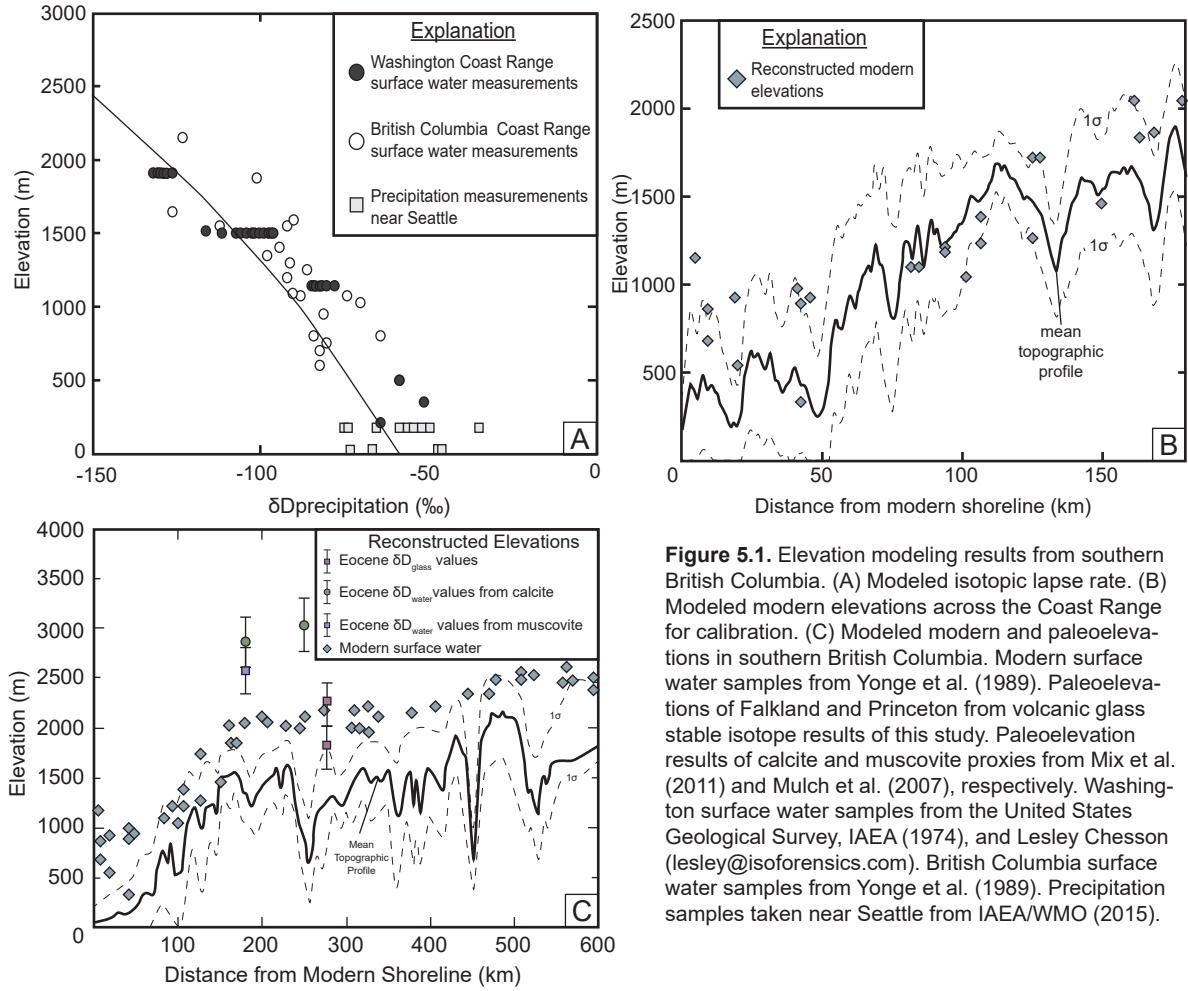





























Figure 5.1. Elevation modeling results from southern British Columbia. (A) Modeled isotopic lapse rate. (B) Modeled modern elevations across the Coast Range for calibration. (C) Modeled modern and paleoelevations in southern British Columbia. Modern surface water samples from Yonge et al. (1989). Paleoelevations of Falkland and Princeton from volcanic glass stable isotope results of this study. Paleoelevation results of calcite and muscovite proxies from Mix et al. (2011) and Mulch et al. (2007), respectively. Washington surface water samples from the United States Geological Survey, IAEA (1974), and Lesley Chesson (lesley@isoforensics.com). British Columbia surface water samples from Yonge et al. (1989). Precipitation samples taken near Seattle from IAEA/WMO (2015).




Appendix 1. White Lake, McAbee Beds, and Hardwick Sandstone Stratigraphy

Explanation		
	Volcaniclastic siltstones, sandstones, and conglomerates	Calculated $\Delta\delta D_{\text{glass}}$ Values (‰)
	Granitic sandstones and conglomerates	
	Carbonaceous claystones, siltstones and sandstones	 -25
	Coal	 -50
	Airfall tephras	 -75
		 -100
		 ≥ -125
		 U/Pb Dating (Zircon)
		 Graded Bedded
		 Ripples
		 Soft sediment deformation
		 Metasequoia
		 Leaves
		 Woody debris






White Lake Formation Lithofacies Descriptions

ID	Color Code	Composition	Sedimentary Features	Corresponding Depositional Environment
WL1		Clast-supported gravel	Weak imbrication, graded bedding	Longitudinal bedforms (high flow regime)
WL2		Clast-supported gravel with sand	Weak grading in sand lenses, weak imbrication	Longitudinal bedforms with scour fills
WL3		Matrix-supported gravel	Weak or no grading	Plastic debris flow
WL4		Sand, fine to very coarse	Solitary or grouped trough cross-beds	Sinuuous-crested and linguoid dunes in channel
WL5		Sand, very fine to coarse	Broad, shallow scours, graded bedding	Scour fills in channel
WL6		Sand, very fine to coarse	Solitary ripple forms with mud drapes, cross lamination	Ripples (lower flow regime)
WL7		Organic-rich sand, very fine to medium	Fine laminations	Overbank or waning flood deposits
WL8		Mud to silt	Fine laminations	Overbank, abandoned channel, or waning flood deposits
WL9		Organic-rich mud to silt	Fine laminations of organic-rich material, soft sedimentary deformation	Backswamp or abandoned channel deposits
WL10		Coal	Bedding thickness ranges from 0.1-2 meters	Vegetated swamp deposits

McAbee Beds Lithofacies Descriptions

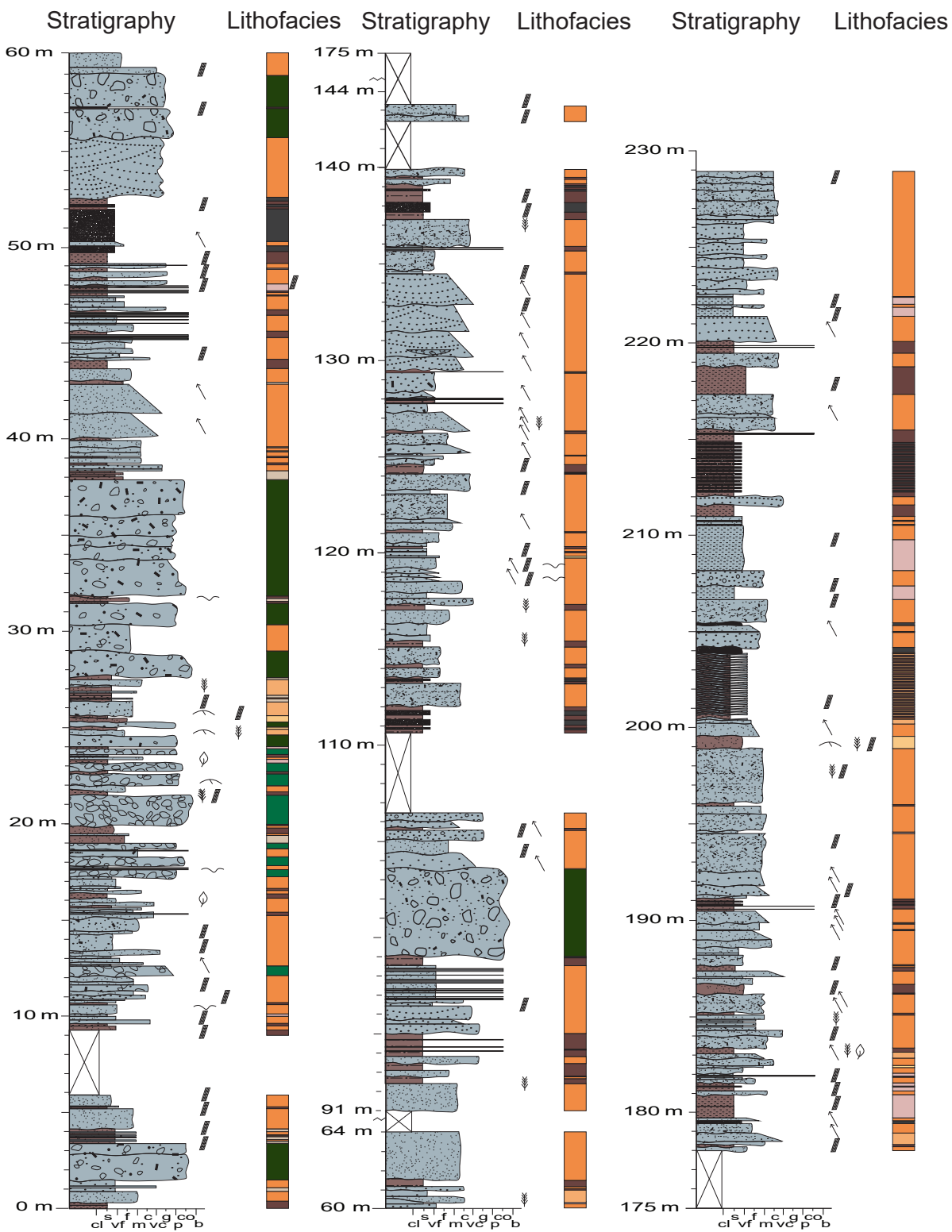
ID	Color Code	Composition	Sedimentary Features	Corresponding Depositional Environment
MB1		Clast-supported gravel	Imbrication, weak grading and gravel lenses	Longitudinal bedforms with scour fills
MB3		Sand, fine to coarse	Graded beds with soft sedimentary deformation	Fluvial-lacustrine (high inflow)
MB2		Organic-rich to organic-poor mud/silt	Weak or no grading and fine lamination	Fluvial-lacustrine

Hardwick Sandstone Lithofacies Descriptions

ID	Color Code	Composition	Sedimentary Features	Corresponding Depositional Environment
PC1		Clast-supported gravel	Weak imbrication and no grading	Longitudinal bedforms (high flow regime)
PC2		Clast-supported gravel	Strong imbrication, weak grading in sand lenses	Longitudinal bedforms with scour fills
PC3		Sand, fine to medium	Broad, shallow scours, graded bedding	Scour fills in channel
PC4		Sand, medium to coarse	Graded beds with mm silt and ash interbeds	Scour fills in channel (low flow)
PC5		Sand, fine to medium	Planar laminations	Plane-bed flow

Appendix 1. White Lake, McAbee Beds, and Hardwick Sandstone Stratigraphy

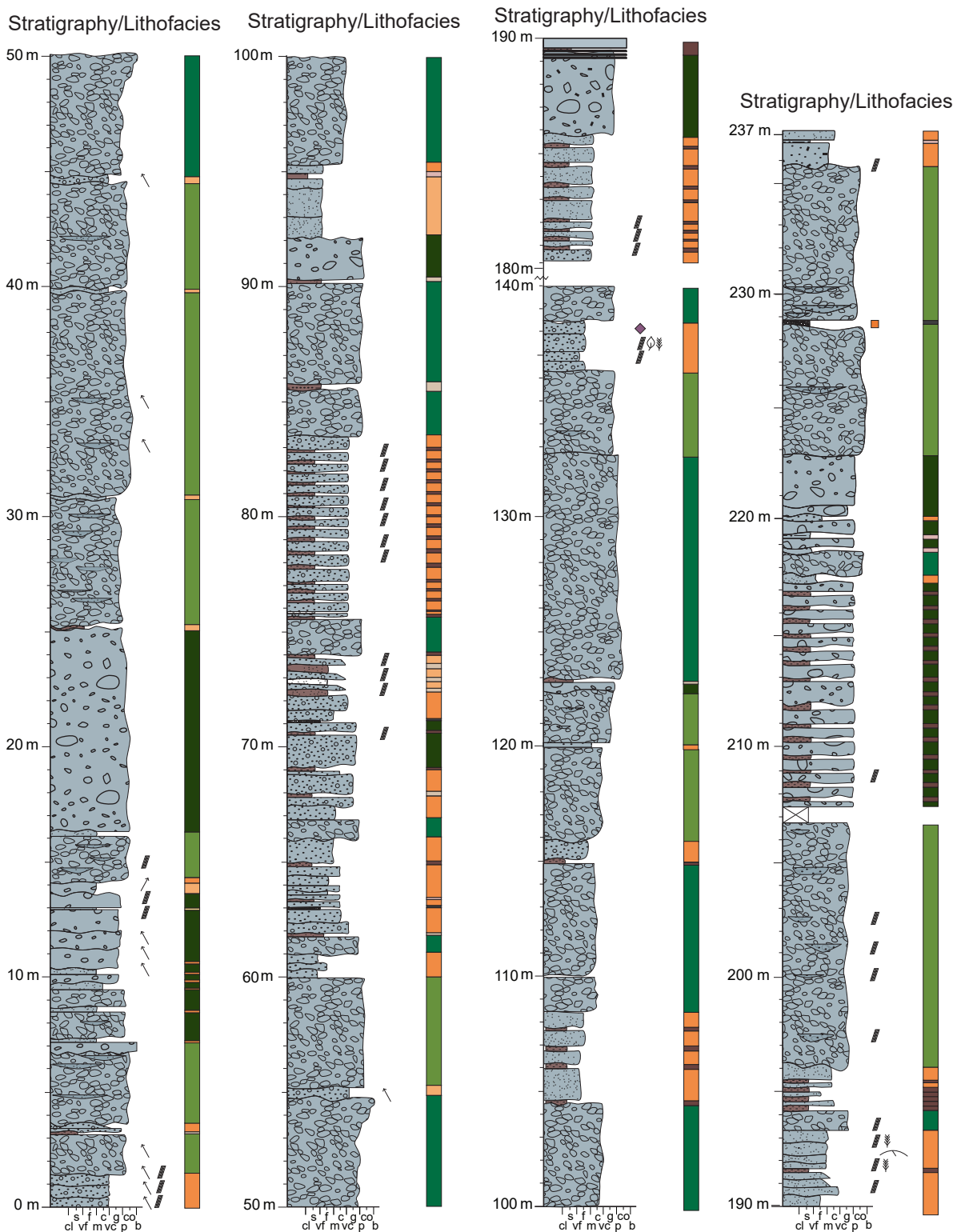
Penticton Group - White Lake Formation
White Lake Road Section



Appendix 1. White Lake, McAbee Beds, and Hardwick Sandstone Stratigraphy

Penticton Group - White Lake Formation

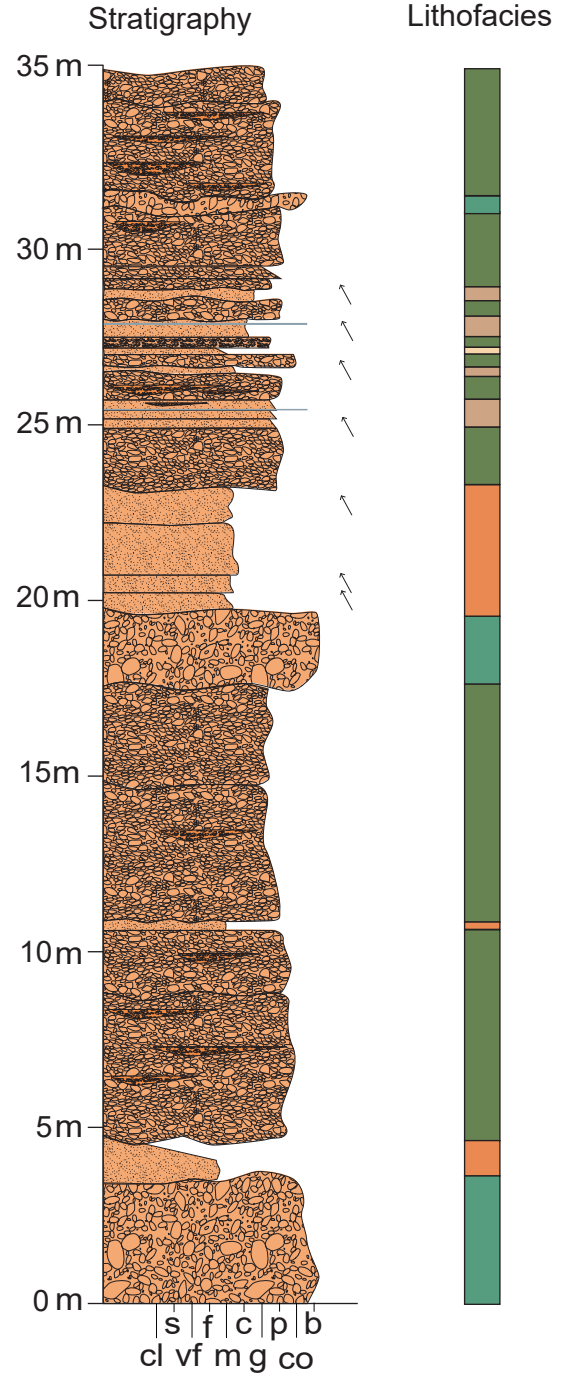
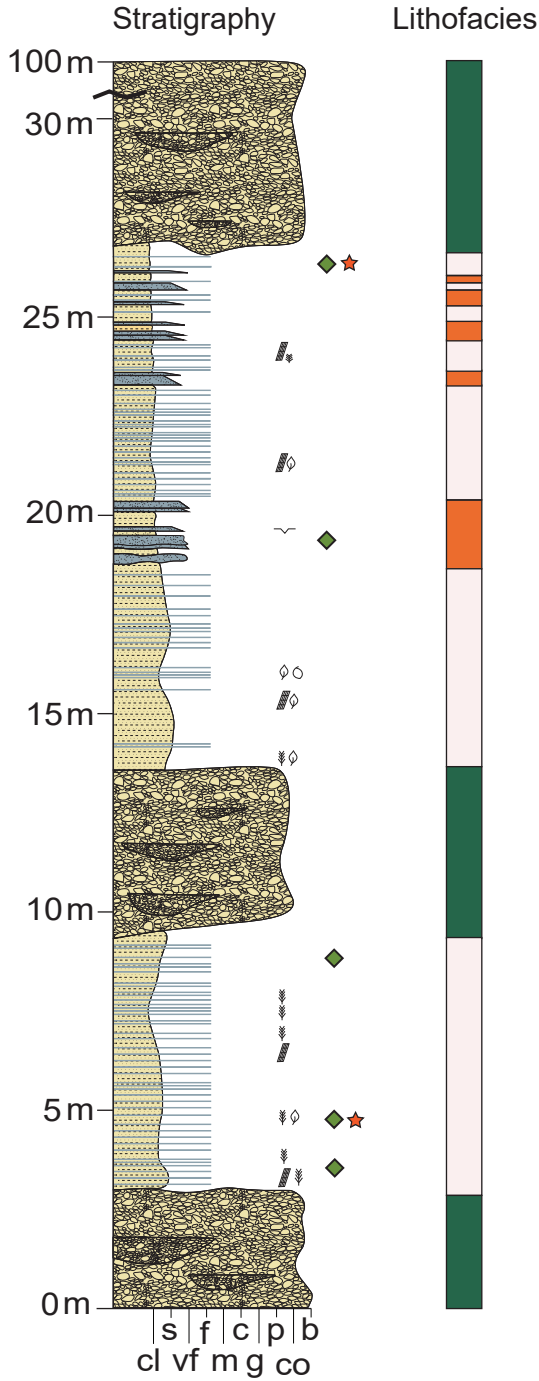
Glenrosa Exit Section



Appendix 1. White Lake, McAbee Beds, and Hardwick Sandstone Stratigraphy

Kamloops Group - Tranquille Formation
 McAbee Beds

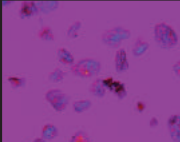
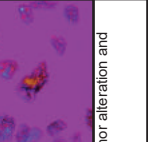
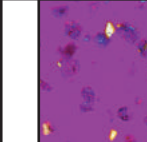
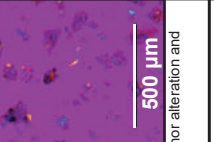
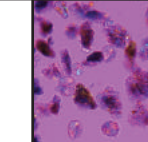
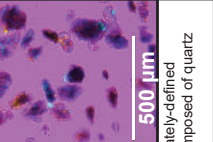
Princeton Group - Allenby Formation
 Hardwick Sandstone Unit
 (Basal Conglomerate)



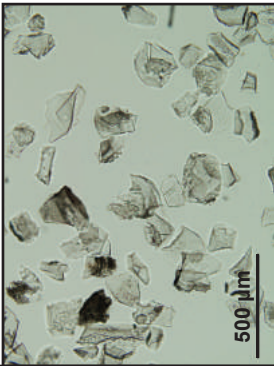
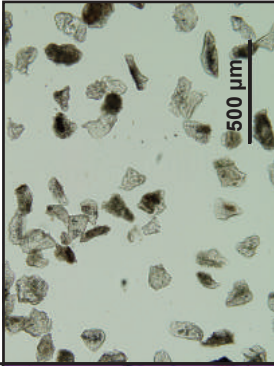
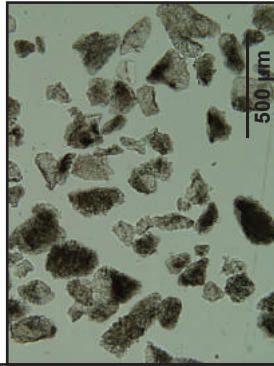
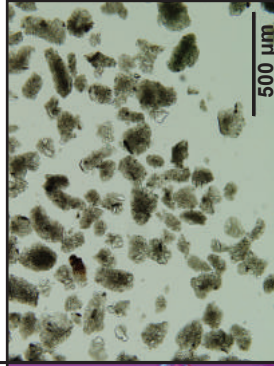
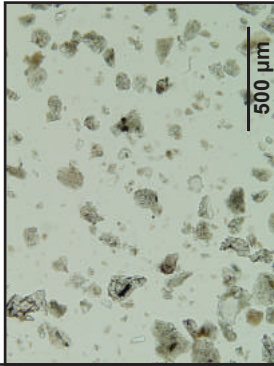
Appendix 2. Full Trace and Rare Earth Element Geochemistry Results

ID	Latitude °N	Longitude °W	EL (m)	Th	Nb	La	Ce	Pr	Nd	Sm	Eu	Gd	Tb	Dy	Ho	Er	Tm	Yb	Lu	Y	Hf	Zr	Ta	U	Pb	Rb	Cs	Sr	Sc	Ba
30FK	50.515	119.632	1387	0.3	1.7	3.4	4.1	0.5	2.0	0.4	0.1	0.4	0.1	0.3	0.1	0.2	0.0	0.2	0.0	2.6	0.4	11.7	0.1	0.7	0.7	5.8	0.4	14.9	0.6	47.4
17PC	49.464	120.512	650	7.6	15.4	25.0	44.6	4.9	16.5	3.0	0.7	1.8	0.2	1.3	0.2	0.6	0.1	0.6	0.1	6.3	1.3	41.6	1.0	1.3	4.9	110.1	11.6	696.9	2.2	1024.9
18PC	49.464	120.512	654	0.8	4.3	2.7	4.6	0.5	1.9	0.3	0.2	0.2	0.0	0.2	0.0	0.1	0.0	0.2	0.0	1.1	1.0	27.7	0.4	0.3	1.8	35.8	3.6	2545.6	2.8	2046.6
33MB(A)	50.797	121.142	609	3.4	2.8	2.7	5.4	0.8	2.9	0.6	0.3	0.3	0.0	0.2	0.0	0.1	0.0	0.2	0.1	1.0	1.3	39.5	0.6	0.3	14.3	38.9	2.6	1447.5	1.2	554.4
34MB(A)	50.797	121.142	609	3.7	7.2	12.4	21.6	2.4	8.6	1.4	0.5	1.0	0.1	0.6	0.1	0.3	0.0	0.4	0.1	3.2	2.3	63.3	1.0	1.1	10.9	49.9	3.5	1035.8	1.8	578.2
39MB	50.797	121.142	609	1.5	3.7	0.8	1.8	0.2	0.7	0.2	0.4	0.2	0.0	0.2	0.0	0.2	0.0	0.3	0.1	1.2	3.1	120.8	0.9	1.0	19.9	42.4	2.4	1084.5	0.3	559.4
63PC	49.563	120.511	770	10.2	8.2	19.8	34.6	3.7	12.1	2.0	0.5	1.1	0.1	0.7	0.1	0.3	0.0	0.3	0.0	3.0	1.3	36.7	0.6	3.2	8.3	99.5	2.9	737.6	1.4	815.3
64PC	49.426	120.554	834	10.5	12.1	33.3	67.9	8.9	35.5	9.8	0.1	10.0	1.8	11.7	2.5	7.0	1.0	6.6	1.0	64.8	8.8	247.7	0.9	4.4	20.8	210.8	6.3	29.9	0.3	98.9
67PC(A)	49.423	120.596	940	1.4	2.6	3.7	8.4	1.1	4.4	1.3	0.1	1.3	0.2	1.7	0.4	1.2	0.2	1.2	0.2	9.6	4.8	122.1	0.5	0.7	11.0	104.3	4.7	305.7	0.3	918.1
73CV	50.148	118.851	1044	9.4	6.5	35.6	58.7	6.1	19.3	3.3	0.9	2.3	0.3	1.9	0.4	1.0	0.1	0.9	0.1	10.3	2.0	74.8	0.9	1.5	10.6	91.4	1.0	246.8	0.7	1696.2
35MB(D)	50.797	121.142	609	8.0	4.9	19.6	31.0	3.1	9.9	1.6	0.4	1.0	0.1	0.8	0.1	0.4	0.1	0.5	0.1	3.9	1.7	53.2	0.9	2.3	4.4	35.9	0.6	266.8	1.4	448.3

Appendix 3. Petrographic Glass Images with Descriptions

<p>BC15-018PC</p>  <p>500 μm</p> <p>This glass separate composition includes 95% glass shards with adhered clays, and quartz inclusions and 5% quartz crystals.</p>	<p>BC15-033MB (A)</p>  <p>500 μm</p> <p>The composition includes 95% glass with minor adhered clays, minor quartz inclusions, minor alteration and poorly- to moderately-defined boundaries. The remainder contains 5% quartz crystals.</p>	<p>BC15-039MB (A)</p>  <p>500 μm</p> <p>The composition includes 95% glass shards with adhered clays, numerous quartz inclusions, and poorly- to moderately-defined boundaries. The remaining composition contains 5% quartz crystals.</p>
<p>BC15-042MB</p>  <p>500 μm</p> <p>The composition includes 90% glass with minor adhered clays, minor quartz inclusions, minor alteration and poorly- to moderately-defined boundaries. The remainder contains 10% quartz crystals.</p>	<p>BC16-073CV</p>  <p>500 μm</p> <p>The glass separate composition includes 95% internally altered glass with poorly-to moderately-defined boundaries and some adhered clays, feldspar and quartz crystals. The remaining 5% is composed of quartz crystals.</p>	<p>BC15-030FK</p>  <p>500 μm</p> <p>The composition includes 95% minimally altered, iron rich, glass shards with poorly-defined boundaries, adhered clays, and minimal quartz inclusions. The remaining 5% completely altered glass shards with poorly-defined crystals, clays, and abundant feldspar and quartz inclusions.</p>

Appendix 3. Petrographic Glass Images with Descriptions

<p>BC16-064PC</p>  <p>500 μm</p> <p>The composition includes 55% glass shards with minimal to no alteration and well-defined boundaries, 45% slighted altered glass with minor adhered clay, minimal quartz inclusions, and well defined crystal boundaries. The remainder contains 5% feldspar crystals.</p>	<p>BC16-067PC (A)</p>  <p>500 μm</p> <p>The g composition includes 95% glass shards, minor adhered clays, and moderate- to well-defined boundaries. The remainder contains 5% quartz and feldspar crystals.</p>
<p>BC16-063PC</p>  <p>500 μm</p> <p>The composition includes 95% glass shards with moderate- to well-defined boundaries, 50% of the glass crystals with minor clay inclusions, moderate quartz inclusions. The remainder consists of 5% quartz crystals.</p>	<p>BC15-017PC</p>  <p>500 μm</p> <p>The composition includes 95% glass shards with altered boundaries, numerous quartz inclusions, and poorly- to moderately-defined boundaries. The remaining compositions contains 5% quartz crystals. Due to alteration and inclusions, we did not consider this sample in this study.</p>
<p>BC15-034MB (A)</p>  <p>500 μm</p> <p>The composition includes 85% glass shards with minor adhered clays, minor quartz inclusions and moderately-defined boundaries. 5% contains altered glass crystals with an abundance of adhered clays, quartz and feldspars. The remainder contains 10% quartz crystals.</p>	

Appendix 4. Full U/Pb Results for Sample BC16-063PC

ID	Lat °N	Long °W	EL (m)	²⁰⁷ Pb/ ²³⁵ U Age (Ma)	1σ Abs Error (Ma)	²⁰⁶ Pb/ ²³⁸ U Age (Ma)	1σ Abs Error (Ma)	²⁰⁷ Pb/ ²⁰⁶ U Age (Ma)	1σ Abs Error (Ma)	²³⁸ Pb/ ²⁰⁶ U Intercept	1σ Abs Error (Ma)	²⁰⁷ Pb/ ²⁰⁶ Pb Average	1σ Abs Error (Ma)	U/Th	U (ppm)	²⁰⁶ Pb/ ²³⁸ U Weight Mean (Ma)	2σ Abs Error (Ma)	MSWD
63PC_52	49.563	120.511	770	47.7	0.9	48.9	0.5	66.4	43.8	131.2	1.4	0.046	0.001	1.5	945.2	50.01	0.41	1.6
63PC_49				51.5	1.0	49.7	0.6	114.5	44.5	129.2	1.4	0.049	0.001	1.5	822.6			
63PC_44				53.1	1.0	50.5	0.6	172.3	43.4	127.1	1.4	0.049	0.001	1.0	993.2			
63PC_43				48.8	1.1	49.4	0.6	21.5	50.9	130.1	1.6	0.046	0.001	1.3	610.0			
63PC_40				55.0	1.1	51.0	0.5	262.5	45.5	125.8	1.3	0.051	0.001	0.8	743.4			
63PC_39				50.4	0.8	50.2	0.6	137.5	45.1	127.8	1.4	0.047	0.001	2.1	1815.4			
63PC_34				50.5	0.9	50.7	0.5	110.3	40.8	126.6	1.4	0.047	0.001	0.8	1015.8			
63PC_33				50.2	0.8	49.4	0.5	129.3	35.5	130.0	1.4	0.048	0.001	0.9	1273.6			
63PC_32				51.3	1.1	50.4	0.6	134.6	58.0	127.3	1.5	0.048	0.001	0.8	674.3			
63PC_31				50.5	1.1	51.0	0.6	80.0	48.5	126.0	1.5	0.047	0.001	1.2	692.1			
63PC_30				53.1	1.0	49.6	0.6	265.5	39.2	129.4	1.5	0.050	0.001	1.0	1104.9			
63PC_29				52.1	1.1	50.1	0.6	223.3	47.3	128.2	1.6	0.049	0.001	1.9	625.9			
63PC_25				47.8	1.1	49.6	0.6	16.0	54.0	129.4	1.5	0.045	0.001	0.9	637.2			
63PC_14				48.0	1.3	48.6	1.0	43.1	52.1	132.1	2.6	0.046	0.001	1.3	697.4			
63PC_13				51.3	1.2	51.6	1.0	88.0	42.0	124.4	2.4	0.047	0.001	1.4	797.0			
63PC_11				50.5	1.1	49.1	0.9	153.4	33.7	130.9	2.5	0.048	0.001	0.7	1576.9			
63PC_9				50.1	1.1	48.2	0.9	153.1	30.0	133.2	2.5	0.049	0.001	1.0	1719.2			
63PC_6				50.3	1.1	48.5	0.9	159.1	32.6	132.3	2.5	0.049	0.001	0.9	2080.8			

Appendix 4. Full U/Pb Results for Sample BC16-064PC

ID	Lat °N	Long °W	EL (m)	²⁰⁷ Pb/ ²³⁵ U Age (Ma)	1σ Abs Error (Ma)	²⁰⁶ Pb/ ²³⁸ U Age (Ma)	1σ Abs Error (Ma)	²⁰⁷ Pb/ ²⁰⁶ Pb Age (Ma)	1σ Abs Error (Ma)	²³⁸ Pb/ ²⁰⁶ U Intercept	1σ Abs Error (Ma)	²⁰⁷ Pb/ ²⁰⁶ Pb Average	1σ Abs Error (Ma)	U/Th	U (ppm)	²⁰⁶ Pb/ ²³⁸ U Weight Mean (Ma)	2σ Abs Error (Ma)	MSWD
64PC_102	49.426	120.554	834	49.0	0.8	47.1	0.5	187.1	34.6	136.5	1.4	0.049	0.001	2.3	1198.9	47.33	0.24	1.18
64PC_99				50.1	0.9	47.0	0.5	209.8	36.9	136.8	1.4	0.050	0.001	1.8	1121.0			
64PC_98				47.1	0.7	47.0	0.4	88.5	28.7	136.7	1.3	0.047	0.001	1.4	2045.7			
64PC_96				46.6	0.8	46.8	0.4	87.8	35.5	137.1	1.3	0.047	0.001	2.0	1248.4			
64PC_93				50.6	0.7	48.1	0.4	168.6	28.1	133.4	1.2	0.049	0.001	1.4	2344.1			
64PC_91				52.7	0.9	47.5	0.6	316.5	30.6	135.1	1.8	0.052	0.001	1.5	1457.0			
64PC_90				51.8	0.8	46.8	0.4	319.8	31.7	137.4	1.3	0.052	0.001	1.7	1532.4			
64PC_87				48.5	0.8	47.8	0.4	87.7	41.2	134.5	1.1	0.048	0.001	2.0	1024.6			
64PC_80				49.5	0.7	48.0	0.4	120.8	30.7	133.8	1.1	0.048	0.001	1.8	1601.6			
64PC_77				47.7	0.8	47.4	0.3	115.5	40.0	135.4	1.0	0.047	0.001	1.9	1210.4			
64PC_76				51.1	0.8	47.7	0.3	214.8	32.6	134.6	1.0	0.050	0.001	1.6	1458.2			
64PC_75				47.5	0.8	47.1	0.4	103.5	39.6	136.3	1.0	0.047	0.001	2.1	1084.7			
64PC_74				49.2	0.8	46.8	0.4	202.9	33.4	137.2	1.1	0.049	0.001	1.7	1444.7			
64PC_73				47.9	0.8	47.1	0.4	112.4	38.1	136.4	1.3	0.048	0.001	1.9	1079.1			
64PC_69				47.4	0.9	47.4	0.7	69.1	33.1	135.5	1.9	0.047	0.001	1.6	1570.3			
64PC_66				51.8	0.9	48.4	0.7	253.7	29.6	132.6	1.9	0.050	0.001	1.7	1720.7			
64PC_65				47.3	0.9	47.2	0.6	92.7	32.0	136.2	1.8	0.047	0.001	1.5	1958.0			
64PC_61				46.0	0.9	46.5	0.6	48.6	33.7	138.1	1.9	0.047	0.001	1.8	1464.8			

Appendix 4. Full U/Pb Results for Sample BC16-067PC(A)

ID	Lat °N	Long °W	EL (m)	²⁰⁷ Pb/ ²³⁵ U Age (Ma)	1σ Abs Error (Ma)	²⁰⁶ Pb/ ²³⁸ U Age (Ma)	1σ Abs Error (Ma)	²⁰⁷ Pb/ ²⁰⁶ U Age (Ma)	1σ Abs Error (Ma)	²³⁸ Pb/ ²⁰⁶ U Intercept	1σ Abs Error (Ma)	²⁰⁷ Pb/ ²⁰⁶ Pb Average	1σ Abs Error (Ma)	U/Th	U (ppm)	²⁰⁶ Pb/ ²³⁸ U Weight Mean (Ma)	2σ Abs Error (Ma)	MSWD
67PC(A)_43	49.423	120.596	940	50.8	0.8	47.5	0.4	215.5	30.0	135.3	1.3	0.050	0.001	1.7	1275.1	48.23	0.26	1.3
67PC(A)_42				56.2	0.9	48.2	0.4	416.8	28.0	133.2	1.2	0.055	0.001	2.0	1380.7			
67PC(A)_41				50.1	0.8	47.8	0.4	166.2	26.3	134.3	1.2	0.049	0.001	1.7	1718.4			
67PC(A)_40				47.4	0.8	47.7	0.4	38.7	30.0	134.6	1.3	0.047	0.001	1.9	1235.6			
67PC(A)_39				48.7	0.8	48.2	0.5	82.8	31.2	133.4	1.3	0.048	0.001	1.9	1435.0			
67PC(A)_38				49.2	0.8	48.0	0.4	110.2	28.2	133.7	1.1	0.048	0.001	2.1	1393.6			
67PC(A)_34				59.3	0.9	47.9	0.4	552.9	27.6	134.0	1.2	0.059	0.001	1.8	1737.4			
67PC(A)_28				49.9	1.4	47.5	0.6	162.3	55.7	135.3	1.7	0.049	0.001	2.1	310.0			
67PC(A)_26				56.0	0.9	48.6	0.5	374.8	29.6	132.0	1.3	0.054	0.001	2.0	1373.3			
67PC(A)_25				50.7	1.6	47.6	0.7	194.8	64.4	135.0	2.0	0.050	0.001	2.2	277.3			
67PC(A)_20				50.4	0.8	47.9	0.4	162.7	28.4	134.1	1.2	0.049	0.001	2.0	1349.7			
67PC(A)_12				49.0	0.7	48.6	0.4	69.8	23.5	132.1	1.1	0.047	0.000	1.3	2835.3			
67PC(A)_11				59.9	1.1	48.4	0.6	549.7	27.9	132.6	1.5	0.059	0.001	1.9	1243.7			
67PC(A)_10				50.4	0.8	48.9	0.4	124.6	27.1	131.3	1.1	0.049	0.001	1.9	1600.8			
67PC(A)_9				47.7	0.8	48.2	0.5	25.5	28.8	133.1	1.4	0.047	0.001	2.0	1300.0			
67PC(A)_8				49.2	0.8	49.4	0.4	40.6	30.4	129.9	1.0	0.047	0.001	2.2	1268.0			
67PC(A)_6				56.1	1.1	48.2	0.5	414.1	34.2	133.3	1.4	0.055	0.001	2.1	1191.1			
67PC(A)_2				51.1	1.0	48.1	0.7	187.7	28.0	133.5	1.9	0.050	0.001	2.1	1522.5			
67PC(A)_1	73.1	1.5	48.4	0.6	976.3	32.1	132.7	1.6	0.072	0.001	1.1	3397.9						

Appendix 4. Full U/Pb Results for Sample BC15-018PC

ID	Lat °N	Long °W	EL (m)	²⁰⁷ Pb/ ²³⁵ U Age (Ma)	1σ Abs Error (Ma)	²⁰⁶ Pb/ ²³⁸ U Age (Ma)	1σ Abs Error (Ma)	²⁰⁷ Pb/ ²⁰⁶ U Age (Ma)	1σ Abs Error (Ma)	²³⁸ Pb/ ²⁰⁶ U Intercept	1σ Abs Error (Ma)	²⁰⁷ Pb/ ²⁰⁶ Pb Average	1σ Abs Error (Ma)	U/Th	U (ppm)	²⁰⁶ Pb/ ²³⁸ U Weight Mean (Ma)	2σ Abs Error (Ma)	MSWD
18PC_48	49.464	120.512	654	49.4	1.0	48.3	0.6	142.5	37.7	132.8	1.7	0.048	0.001	2.0	1184.3	48.18	0.35	1.2
18PC_44				48.1	0.9	47.5	0.6	687.4	95.5	135.2	1.7	0.048	0.001	1.9	1310.0			
18PC_39				48.6	0.9	48.6	0.6	111.1	33.4	132.2	1.6	0.047	0.001	1.8	1437.6			
18PC_38				54.8	1.0	48.0	0.6	417.4	32.2	133.7	1.7	0.054	0.001	1.8	1317.6			
18PC_37				48.9	0.9	48.0	0.6	136.1	32.1	133.8	1.6	0.048	0.001	1.6	1773.2			
18PC_36				46.7	0.9	47.0	0.6	70.6	37.3	136.7	1.8	0.047	0.001	1.8	1093.2			
18PC_35				46.5	0.9	46.9	0.7	82.8	40.0	136.9	1.9	0.047	0.001	1.6	1160.2			
18PC_27				58.8	1.0	47.6	0.5	569.4	31.6	134.8	1.4	0.058	0.001	1.7	1586.0			
18PC_24				52.5	1.0	48.6	0.7	230.7	34.6	132.1	1.8	0.051	0.001	1.3	1274.1			
18PC_21				50.1	0.8	48.9	0.6	143.5	27.1	131.3	1.6	0.048	0.001	1.1	2588.4			
18PC_20				49.8	0.9	48.6	0.6	184.4	37.7	132.2	1.5	0.048	0.001	2.0	1295.1			
18PC_14				49.2	1.0	47.8	0.7	145.1	32.3	134.2	1.9	0.048	0.001	1.7	1731.0			
18PC_13				49.8	1.0	48.1	0.7	185.7	39.5	133.6	2.0	0.049	0.001	2.0	1237.9			
18PC_11				52.5	1.0	49.6	0.7	656.5	344.9	129.4	1.9	0.050	0.001	1.8	1568.7			
18PC_10				49.8	0.9	48.4	0.7	106.3	31.4	132.7	1.8	0.048	0.001	1.7	1764.8			
18PC_7				49.5	0.9	48.8	0.6	129.4	31.7	131.6	1.7	0.048	0.001	1.8	1651.0			
18PC_5	50.6	0.8	48.8	0.6	165.5	29.8	131.6	1.6	0.049	0.001	1.2	2973.4						

Appendix 4. Full U/Pb Results for Sample BC15-034MB(A)

ID	Lat °N	Long °W	EL (m)	²⁰⁷ Pb/ ²³⁵ U Age (Ma)	1σ Abs Error (Ma)	²⁰⁶ Pb/ ²³⁸ U Age (Ma)	1σ Abs Error (Ma)	²⁰⁷ Pb/ ²⁰⁶ U Age (Ma)	1σ Abs Error (Ma)	²³⁸ Pb/ ²⁰⁶ U Intercept	1σ Abs Error (Ma)	²⁰⁷ Pb/ ²⁰⁶ Pb Average	1σ Abs Error (Ma)	U/Th	U (ppm)	²⁰⁶ Pb/ ²³⁸ U Weight Mean (Ma)	2σ Abs Error (Ma)	MSWD
34MB (A)_37	50.797	121.142	609	51.8	0.9	50.8	0.7	110.0	23.5	126.4	1.8	0.048	0.000	2.7	2976.0	51.00	0.31	1.09
34MB (A)_34				56.0	1.2	51.8	0.8	310.8	47.4	123.9	1.9	0.051	0.001	1.4	792.2			
34MB (A)_32				52.1	1.0	52.0	0.8	98.5	31.4	123.4	1.8	0.047	0.001	1.6	1651.2			
34MB (A)_29				54.0	1.0	51.0	0.7	190.1	23.2	125.9	1.8	0.050	0.000	1.2	2204.5			
34MB (A)_27				55.8	1.6	51.5	0.9	396.4	59.7	124.6	2.1	0.051	0.001	0.9	340.3			
34MB (A)_26				52.5	0.9	50.9	0.7	125.2	18.2	126.2	1.9	0.049	0.000	1.8	6979.2			
34MB (A)_25				54.1	1.0	51.9	0.8	166.7	30.4	123.6	1.8	0.049	0.001	0.9	2386.1			
34MB (A)_21				54.3	1.0	50.9	0.6	233.2	35.8	126.2	1.5	0.050	0.001	2.3	968.2			
34MB (A)_19				50.9	0.7	50.4	0.5	72.2	20.8	127.3	1.3	0.048	0.000	1.7	5061.2			
34MB (A)_18				52.8	0.7	51.9	0.5	105.4	19.1	123.8	1.2	0.048	0.000	2.4	5989.3			
34MB (A)_17				50.9	0.7	50.5	0.5	70.2	21.0	127.2	1.4	0.047	0.000	1.2	4522.0			
34MB (A)_16				51.0	0.9	49.5	0.6	441.4	34.6	129.7	1.6	0.049	0.001	3.0	2024.9			
34MB (A)_14				52.3	0.8	51.1	0.5	106.4	25.9	125.7	1.3	0.048	0.001	2.4	2300.9			
34MB (A)_11				52.1	1.0	50.5	0.6	179.0	38.0	127.1	1.5	0.049	0.001	1.9	803.0			
34MB (A)_10				51.2	0.9	51.2	0.7	57.6	22.9	125.4	1.7	0.047	0.000	1.9	3467.5			
34MB (A)_7				53.0	1.1	51.7	0.8	114.8	26.7	124.2	2.0	0.048	0.001	1.8	1806.8			
34MB (A)_2				64.3	1.4	51.1	0.8	589.6	33.7	125.6	2.0	0.060	0.001	0.9	845.2			

Appendix 4. Full U/Pb Results for Sample BC15-039MB

ID	Lat °N	Long °W	EL (m)	²⁰⁷ Pb/ ²³⁵ U Age (Ma)	1σ Abs Error (Ma)	²⁰⁶ Pb/ ²³⁸ U Age (Ma)	1σ Abs Error (Ma)	²⁰⁷ Pb/ ²⁰⁶ U Age (Ma)	1σ Abs Error (Ma)	²³⁸ Pb/ ²⁰⁶ U Intercept	1σ Abs Error (Ma)	²⁰⁷ Pb/ ²⁰⁶ Pb Average	1σ Abs Error (Ma)	U/Th	U (ppm)	²⁰⁶ Pb/ ²³⁸ U Weight Mean (Ma)	2σ Abs Error (Ma)	MSWD
39MB_100	50.797	121.142	609	51.8	1.0	50.1	0.6	137.3	42.3	128.1	1.6	0.049	0.001	1.1	792.8	50.80	0.34	1.4
39MB_99				51.6	0.9	50.8	0.6	97.0	32.5	126.5	1.5	0.048	0.001	0.9	1294.0			
39MB_93				52.8	0.9	51.2	0.6	136.6	33.3	125.4	1.5	0.049	0.001	1.0	1216.7			
39MB_92				56.4	1.0	51.1	0.6	348.7	34.7	125.7	1.6	0.052	0.001	1.0	1089.4			
39MB_150				52.8	1.3	50.4	0.6	320.6	67.7	127.4	1.4	0.049	0.001	1.3	449.9			
39MB_149				51.5	0.9	51.2	0.5	121.7	41.9	125.5	1.2	0.047	0.001	1.1	980.7			
39MB_147				49.7	1.1	50.2	0.6	93.6	54.3	128.0	1.5	0.047	0.001	1.2	465.1			
39MB_146				53.5	0.9	50.2	0.5	215.1	38.0	127.9	1.3	0.050	0.001	0.7	1071.9			
39MB_143				54.3	1.3	51.1	0.6	238.9	59.9	125.7	1.5	0.050	0.001	1.2	446.7			
39MB_142				63.0	1.5	52.1	0.7	544.9	52.4	123.3	1.6	0.057	0.001	1.1	401.2			
39MB_141				55.3	1.1	50.2	0.5	311.9	47.9	127.9	1.4	0.052	0.001	0.9	626.6			
39MB_138				50.4	0.7	50.2	0.5	65.6	31.0	128.0	1.2	0.047	0.001	0.9	1799.9			
39MB_137				49.8	1.0	50.0	0.5	71.7	51.2	128.4	1.4	0.047	0.001	1.1	585.2			
39MB_136				49.9	1.4	51.0	0.6	64.3	74.8	126.0	1.5	0.046	0.001	1.2	360.4			
39MB_135				50.4	0.8	51.7	0.4	20.8	39.2	124.2	1.1	0.046	0.001	1.2	1069.5			
39MB_134				53.2	0.8	51.4	0.4	152.9	34.2	124.9	1.1	0.049	0.001	1.1	1248.9			

Appendix 4. Full U/Pb Results for Sample BC16-043RP

ID	Lat °N	Long °W	EL (m)	²⁰⁷ Pb/ ²³⁵ U Age (Ma)	1σ Abs Error (Ma)	²⁰⁶ Pb/ ²³⁸ U Age (Ma)	1σ Abs Error (Ma)	²⁰⁷ Pb/ ²⁰⁶ U Age (Ma)	1σ Abs Error (Ma)	²³⁸ Pb/ ²⁰⁶ U Intercept	1σ Abs Error (Ma)	²⁰⁷ Pb/ ²⁰⁶ Pb Average	1σ Abs Error (Ma)	U/Th	U (ppm)	²⁰⁶ Pb/ ²³⁸ U Weight Mean (Ma)	2σ Abs Error (Ma)	MSWD
43RP_61	48.615	118.733	687	50.3	1.6	52.2	0.6	63.7	76.7	123.1	1.4	0.045	0.001	0.9	297.4	52.43	0.55	1.6
43RP_58				58.5	2.0	52.2	0.7	501.2	77.2	122.9	1.7	0.053	0.002	1.0	212.1			
43RP_52				68.9	2.4	53.7	0.8	848.4	78.1	119.6	1.7	0.061	0.002	0.9	198.0			
43RP_51				62.8	2.4	53.0	0.8	579.0	81.3	121.2	1.9	0.056	0.002	1.0	173.6			
43RP_46				55.1	1.6	52.0	0.6	283.3	70.3	123.4	1.3	0.050	0.001	0.8	352.2			
43RP_40				78.0	2.3	52.5	0.7	1108.4	65.6	122.3	1.7	0.071	0.002	0.5	246.0			
43RP_38				63.2	1.8	53.7	0.6	455.4	63.6	119.6	1.4	0.056	0.002	1.4	328.6			
43RP_32				49.3	1.8	51.8	0.8	213.2	103.4	123.9	1.8	0.045	0.002	0.9	263.8			
43RP_29				51.3	1.4	51.7	0.7	129.3	65.3	124.3	1.6	0.047	0.001	0.6	438.8			
43RP_27				51.9	1.7	50.6	0.7	184.7	74.9	126.8	1.8	0.048	0.002	0.9	302.1			
43RP_26				54.8	1.8	53.4	0.8	280.7	72.7	120.2	1.7	0.048	0.001	0.8	264.2			
43RP_25				55.1	1.4	52.8	0.7	253.9	57.6	121.5	1.5	0.049	0.001	1.0	518.8			

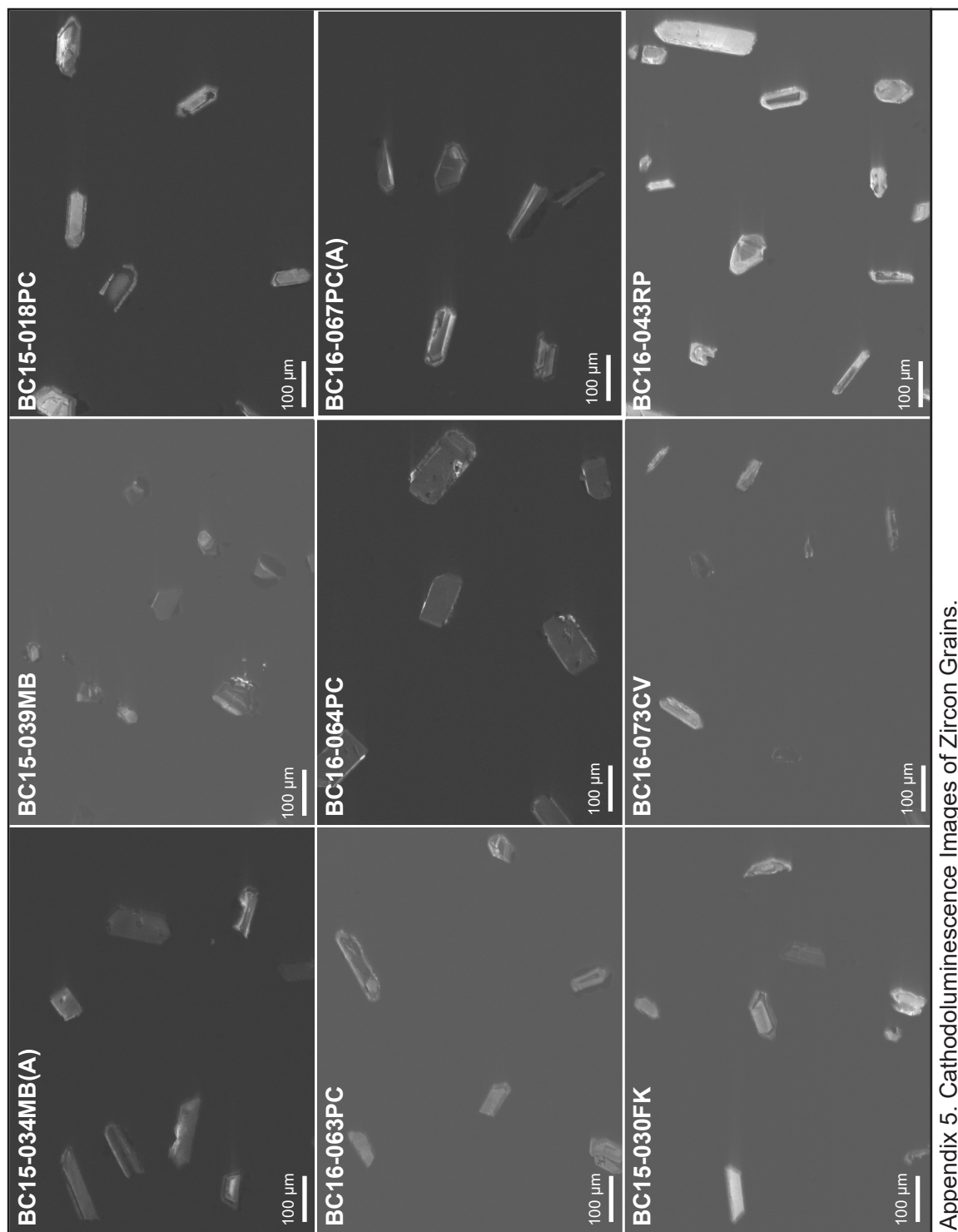
Appendix 4. Full U/Pb Results for Sample BC15-030FK

ID	Lat °N	Long °W	EL (m)	²⁰⁷ Pb/ ²³⁵ U Age (Ma)	1σ Abs Error (Ma)	²⁰⁶ Pb/ ²³⁸ U Age (Ma)	1σ Abs Error (Ma)	²⁰⁷ Pb/ ²⁰⁶ U Age (Ma)	1σ Abs Error (Ma)	²³⁸ Pb/ ²⁰⁶ U Intercept	1σ Abs Error (Ma)	²⁰⁷ Pb/ ²⁰⁶ Pb Average	1σ Abs Error (Ma)	U/Th	U (ppm)	²⁰⁶ Pb/ ²³⁸ U Weight Mean (Ma)	2σ Abs Error (Ma)	MSWD
30FK_66	50.515	119.632	1387	53.9	1.7	51.9	0.9	455.9	44.0	123.7	2.1	0.049	0.001	2.4	666.0	50.20	1.00	2.7
30FK_65				78.6	3.1	51.2	1.0	1259.0	79.2	125.5	2.4	0.073	0.003	0.9	134.8			
30FK_64				77.3	3.1	52.0	1.0	1257.4	84.7	123.4	2.3	0.071	0.003	0.6	161.7			
30FK_63				48.6	0.8	48.4	0.6	57.2	34.0	132.6	1.5	0.047	0.001	0.9	1657.0			
30FK_62				56.9	1.9	50.4	0.8	491.5	75.6	127.3	2.0	0.053	0.002	0.8	273.5			
30FK_61				67.5	2.8	51.6	0.9	846.7	106.8	124.4	2.3	0.062	0.003	0.8	155.6			
30FK_60				57.7	1.2	49.7	0.7	1390.4	50.5	129.3	1.7	0.055	0.001	0.7	1490.0			
30FK_59				49.3	1.9	50.4	1.0	848.4	106.5	127.3	2.6	0.046	0.002	0.4	244.4			
30FK_58				51.6	2.1	50.0	1.0	1932.2	86.3	128.6	2.7	0.049	0.002	0.4	245.3			

Appendix 4. Full U/Pb Results for Sample BC16-073CV

ID	Lat °N	Long °W	EL (m)	²⁰⁷ Pb/ ²³⁵ U Age (Ma)	1σ Abs Error (Ma)	²⁰⁶ Pb/ ²³⁸ U Age (Ma)	1σ Abs Error (Ma)	²⁰⁷ Pb/ ²⁰⁶ U Age (Ma)	1σ Abs Error (Ma)	²³⁸ Pb/ ²⁰⁶ U Intercept	1σ Abs Error (Ma)	²⁰⁷ Pb/ ²⁰⁶ Pb Average	1σ Abs Error (Ma)	U/Th	U (ppm)	²⁰⁶ Pb/ ²³⁸ U Weight Mean (Ma)	2σ Abs Error (Ma)	MSWD
73CV_86	50.148	118.851	1044	90.0	1.9	50.4	0.6	3082.9	49.2	127.5	1.6	0.086	0.002	1.1	1543.5	50.14	0.91	2.4
73CV_82				49.4	0.7	49.1	0.5	90.1	30.3	130.9	1.4	0.047	0.001	1.9	2169.7			
73CV_78				67.0	0.9	49.4	0.5	802.5	27.5	129.9	1.3	0.064	0.001	0.4	1802.9			
73CV_77				51.6	0.7	50.3	0.5	109.7	21.1	127.6	1.3	0.048	0.000	1.3	6020.4			
73CV_76				58.0	1.9	51.2	0.9	397.0	51.4	125.3	2.2	0.053	0.002	0.8	394.4			
73CV_74				66.3	0.9	51.2	0.5	900.6	32.5	125.5	1.2	0.061	0.001	0.6	3310.2			

Appendix 5. Cathodoluminescence Images of Zircon Grains



Appendix 5. Cathodoluminescence Images of Zircon Grains.